

Article

Leader–Follower Formation Tracking Control of Underactuated Surface Vehicles Based on Event-Triggered Control

Xiaoming Xia * , Zhaodi Yang and Tianxiang Yang

School of Ocean Engineering, Jiangsu Ocean University, Lianyungang 222005, China; yangzhaodi@jou.edu.cn (Z.Y.); yangtx_7@126.com (T.Y.)

* Correspondence: xia_xm@126.com

Abstract: This paper investigates the leader–follower formation tracking control of underactuated surface vessels (USVs) with input saturation. Each vessel is subject to the uncertainties induced by model uncertainties and environmental disturbances. First, an event-triggered extended-state observer (ETESO) is used to recover the velocity, yaw rate and uncertainties. Then, an estimator is used to estimate the velocity of the leader. An event-triggered controller (ETC) is constructed based on the estimator, the observer and extra variables. Specifically, extra variables are used to solve the problems of underactuation and input saturation. Stability analysis of the control system is conducted to prove that all signals are bounded. Simulations demonstrate that the ETESO can accurately estimate the uncertainties, velocity and yaw rate, and the ETC can largely reduce the action times of actuator.

Keywords: leader–follower; event-triggered controller; underactuated surface vessels; formation tracking



Citation: Xia, X.; Yang, Z.; Yang, T. Leader–Follower Formation Tracking Control of Underactuated Surface Vehicles Based on Event-Triggered Control. *Appl. Sci.* **2023**, *13*, 7156. <https://doi.org/10.3390/app13127156>

Academic Editor: Atsushi Mase

Received: 16 May 2023

Revised: 9 June 2023

Accepted: 10 June 2023

Published: 15 June 2023



Copyright: © 2023 by the authors. Licensee MDPI, Basel, Switzerland. This article is an open access article distributed under the terms and conditions of the Creative Commons Attribution (CC BY) license (<https://creativecommons.org/licenses/by/4.0/>).

1. Introduction

In recent years, formation tracking control of underactuated surface vessels (USVs) has attracted considerable interest, as USVs can be widely used in ocean engineering fields [1–3]. Compared with single vessels, formations offer many advantages. In the course of ocean exploration, the efficiency of a single vessel is low, whereas formations can perform the complex tasks such as pursuit tasks that usually cannot be accomplished by a single vessel. There are various formation control schemes, including the leader–follower approach [4,5], virtual structure [6], the graph-based mechanism [7], the data-driven model [8], UAV–USV heterogeneous multiagent systems [9] and adaptive fuzzy formation control [10]. In particular, the leader–follower strategy is preferred in ocean engineering applications. The follower maintains a desired distance and angle relative to the leader, and a reference trajectory can be defined by the leader. Therefore, the group behavior is directed by the leader, and the formation stability can be induced by the control law of a single vessel.

There are two main challenges that are still worth mentioning. The first challenge is actuator saturation, which can severely degrade the closed-loop system performance [11]. In practice, each actuator of a vessel can only provide a limited force or torque. To reduce the risk of actuator saturation and enhance system performance, some methods have been proposed in recent years. To avoid poor tracking performance in formation control, generalized saturation functions combined with formation tracking errors were employed to handle the input saturation problem [12]. To solve the problems of input saturation and underactuation simultaneously, additional variables were induced to velocity errors in the body-fixed frame [13,14]. Non-linear saturation of an actuator was approximated by a Gaussian error function [15] such that an anti-saturation controller could be designed. An auxiliary dynamic system was constructed to solve the input saturation problem [16], with the auxiliary dynamic system designed as a second-order system, providing a conservative

input signal. A first-order auxiliary system was designed in [17] and employed to deal with input saturation of the rudder. The authors of [18] used an auxiliary system to solve the problem of input saturation, which was combined with a collision-avoidance control strategy to provide tracking control for dynamic vessel positioning. However, the limited acting frequency actuators was not considered in the articles mentioned above.

High-frequency action may lead not only to mechanical abrasion but also to a short service life [19]. Input saturation and actuator rate limits were considered in [20], and a non-linear controller was designed based on dynamic surface control and backstepping technology. Additional controllers were proposed to deal with actuator magnitude and rate saturation in [21]. The authors of [22] considered actuator saturation with limited magnitude and rate and designed a sliding model controller. In [20–22], Zeno behavior was avoided because the acting frequency of actuator was bounded. A controller combined with an event-triggered condition was proposed in [23], and the triggered condition was designed based on the flow time and error function; however, this configuration still resulted in long action times of the actuator. An event-triggered distributed controller was employed in [24], and the triggered condition was designed based on changes in amplitude of input signals. The authors of [25] proposed an event-triggered control law, and an event-triggered mechanism was used to reduce the execution frequency of actuators. The event-triggered mechanism was designed in the controller-to-actuator channel, and the execution rate of the actuator was reduced.

The second significant challenge is the uncertainties. Because of the working condition of the surface vessel, uncertainties include model uncertainties and environmental disturbances. In [26], the proposed controller was robust to the parameter uncertainties of the nonlinear terms and exogenous disturbances. Unknown plant parameters and environmental disturbances were solved using parameter estimation and upper-bound estimation in [27]. In [28], a robust adaptive control algorithm was proposed to solve uncertain parameters. Adaptive estimators were designed to estimate unknown time-varying functions of vessel model in [29]. Considering the leader–follower formation tracking problem, a neural network was used to approximate the uncertainties, and the uncertainties were compensated by online learning [30]. A cooperative controller was proposed using position-heading measurements in [31], and an extended-state observer (ESO) was constructed to provide the estimations of velocity, yaw rate and uncertainties. However, the existing observers presented in [14,16,19,25,31,32] relied on continuous sampling. In each execution cycle, signals are transmitted, which means that many network resources and calculation resources are consumed. To avoid unnecessary calculation and communication, an event-triggered extended-state observer (ETESO) was proposed in [33]. In [34], an ETESO was proposed for a class of non-linear networked control systems, and the state estimation problem was solved. As for USVs, when the working mode is tracking control, in most cases, the yaw angle is unchanged. In the common continuous observer, the signals have to be transmitted during each execution cycle, consuming many network resources and calculation resources. Therefore, it is rewarding to design a leader–follower tracking controller with a light transmission load and short action times of actuators.

Based on the above research background, in this paper, we investigate leader–follower formation tracking control of USVs subject to input saturation, model uncertainties and environmental disturbances. Inspired by the work reported in [23,31], an improved output feedback controller was proposed. First, an ETESO was used to recover the velocity data and model uncertainties and disturbances. In each execution cycle, an event-triggered strategy is monitored to determine whether or not to transmit the position and head information to the observer. Sensor-to-observer communication costs are drastically reduced. Secondly, an estimator is employed to estimate the velocity of the leader and reduce the amount of data exchanged in formation. Thirdly, auxiliary variables provide a solution for the problems of input saturation and underactuation. Then, an event-triggered controller (ETC) was designed based on the ETESO, the estimator and auxiliary variables. Finally,

the stability of the closed-loop system was proven. Simulations were also conducted to demonstrate the proposed control strategy.

Two salient features of the proposed control are summarized as follows. First, an estimator is employed to estimate the velocity of the leader, the embedded processor of each follower performs reading computations only using the position and yaw of the leader and the transmission loads between formations are saved. Second, an event-triggered mechanism is designed in the controller-to-actuator channel, and action times of actuator are reduced.

Compared with the existing related results, the novelty of this paper is summarized as follows. First, in contrast to existing formation control approaches [25,31], the velocity of the leader is estimated by an estimator, which reduces the amount of data exchanged between USVs. Second, compared with the observer proposed in [31], the ETESO can reduce sensor-to-observer communication costs. Third, compared with the strategy proposed in [23], the proposed control law can largely reduce the action times of the actuator.

The remainder of this paper is organized as follows. A list of notations defining variables used in this paper is presented in Table 1. Section 2 describes the preliminaries and problem formulation. Section 3 describes observer design, and Section 4 presents the controller design and a stability analysis. Simulation results are presented in Section 5. Section 6 concludes this paper.

Table 1. Notations and variables used in this paper.

\mathbb{R}^n	n -dimensional Euclidean space
$ \cdot $	Absolute value of a variable
$\lambda_{\min}(\cdot)$	Minimum eigenvalue of a matrix
$\min\{\cdot\}$	Minimum value of a set
$\inf\{\cdot\}$	Supremum of a set
$(\cdot)^T$	Transpose of a matrix
$\ \cdot\ $	Euclidean norm of a vector
$\text{diag}\{\cdot\}$	Diagonal matrix
I_n	$n \times n$ dimensional identity matrix
0_n	$n \times n$ dimensional zero matrix.
$(x_i, y_i), \psi_i, (x_j, y_j), \psi_j$	Position and yaw of the i th USV and the leader (j)
$u_i, v_i, r_i, u_j, v_j, r_j$	Surge velocity, sway velocity and yaw rate of the i th USV and the leader (j)
$m_{i,11}, m_{i,22}, m_{i,33}$	Inertia mass of the i th USV
$\sigma_{i,h}$	Hydrodynamic damping parameters and disturbances
$\tau_i = [\tau_{i,u}, 0, \tau_{i,r}]$	Input signals of the i th USV
η_i, v_i	$\eta_i = [x_i, y_i, \psi_i]^T, v_i = [u_i, v_i, r_i]^T$
η_j, v_j	$\eta_j = [x_j, y_j, \psi_j]^T, v_j = [u_j, v_j, r_j]^T$
M_i	$M_i = \text{diag}\{m_{i,11}, m_{i,22}, m_{i,33}\}$
R_i	Rotation matrices of the i th USV
$\tau_{ic} = [\tau_{i,uc}, 0, \tau_{i,rc}]^T$	τ_{ic} calculated by the proposed controller
$\omega_i = [\omega_{i,u}, 0, \omega_{i,r}]^T$	The mismatch function between input without saturation and input with saturation
ρ_{ij}, λ_{ij}	Relative distance and angle between the i th USV and the leader (j)
$\rho_{ij,d}, \lambda_{ij,d}$	Desired distance and angle
\hat{x}	Estimate of variable x
t_k	Previous event-triggering time instant
ξ_i	Transmitted signal between $\eta_i(t)$ and $\eta_i(t_k)$
$d(t)$	Event-triggered mechanism
$\tilde{x} = \hat{x} - x$	Estimation error of variable x
$P_{ij} = [\rho_{ij,e}, \lambda_{ij,e}]^T$	Formation tracking error vector
$\hat{\Theta}_i$	Estimator used to estimate velocity of the leader
$l_{i,h}$	Time constants of the first-order filters
$\psi_{i,e}$	Yaw tracking error
$\beta_{i,h}$	Virtual controls

Table 1. Cont.

$\alpha_{i,h}$	Auxiliary variables
$\omega_{i,h}$	Errors caused by the first-order filter
$\omega_{\tau u}, \omega_{\tau r}$	Control laws at the kinetic level

2. Problem Formulation

As shown in Figure 1, a group of USVs consists of N USVs, and the model of the i th USV is given as [35]

$$\dot{x}_i = u_i \cos(\psi_i) - v_i \sin(\psi_i), \tag{1}$$

$$\dot{y}_i = u_i \sin(\psi_i) + v_i \cos(\psi_i), \tag{2}$$

$$\dot{\psi}_i = r_i, \tag{3}$$

and

$$\dot{u}_i = \sigma_{i,1} + \frac{1}{m_{i,11}} \tau_{i,u}, \tag{4}$$

$$\dot{v}_i = \sigma_{i,2}, \tag{5}$$

$$\dot{r}_i = \sigma_{i,3} + \frac{1}{m_{i,33}} \tau_{i,r}, \tag{6}$$

where $(x_i, y_i)^T \in \mathbb{R}^2$ is the position in the Earth-fixed frame ($X_E O_E Y_E$); ψ_i is the yaw angle in $X_E O_E Y_E$; u_i is the surge velocity in the body-fixed frame ($X_B O_B Y_B$); v_i is the sway velocity in $X_B O_B Y_B$; r_i is the yaw rate in $X_B O_B Y_B$; $m_{i,11}$ and $m_{i,33}$ denote the inertia mass; uncertainties $\sigma_{i,1}$, $\sigma_{i,2}$ and $\sigma_{i,3}$ contain Coriolis parameters, hydrodynamic damping parameters and time-varying disturbances, respectively; and $\tau_{i,u}$ and $\tau_{i,r}$ are input signals.

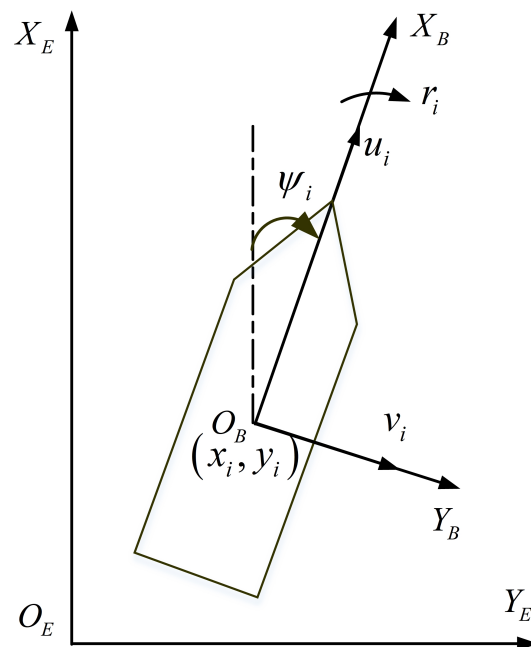


Figure 1. Earth-fixed frame and body-fixed frame.

To facilitate observer design and analysis, the i th USV model is written as

$$\dot{\eta}_i = R_i v_i \tag{7}$$

$$v_i = M_i^{-1} \tau_i + \sigma_i, \tag{8}$$

where $\eta_i = [x_i, y_i, \psi_i]^T$, $v_i = [u_i, v_i, r_i]^T$, $\tau_i = [\tau_{i,u}, 0, \tau_{i,r}]^T$, $M_i = \text{diag}\{m_{i,11}, m_{i,22}, m_{i,33}\}$, $m_{i,22}$ is the inertia mass. $\sigma_i = [\sigma_{i,1}, \sigma_{i,2}, \sigma_{i,3}]^T$, and

$$R_i = \begin{bmatrix} \cos(\psi_i) & -\sin(\psi_i) & 0 \\ \sin(\psi_i) & \cos(\psi_i) & 0 \\ 0 & 0 & 1 \end{bmatrix}.$$

The mismatch function between input without saturation and input with saturation is described as $\omega_i = [\omega_{i,u}, 0, \omega_{i,r}]^T = \tau_{ic} - \tau_i$, where $\tau_{ic} = [\tau_{i,uc}, 0, \tau_{i,rc}]^T$; $\tau_{i,uc}$ and $\tau_{i,rc}$ are the surge force and yaw moment calculated by the proposed controller, respectively; and $\tau_i = [\tau_{i,u}, 0, \tau_{i,r}]^T$. Then, the saturated control is given by $\tau_i = \tau_{ic} - \omega_i$.

Assumption 1. The unknown function σ_i satisfies $\dot{\sigma}_i \leq \sigma_i^*$, where σ_i^* is a positive constant.

σ_i is a vector containing velocity, Coriolis parameters, hydrodynamic damping parameters and time-varying disturbances. It is natural to assume that their derivatives are bounded. Control inputs to drive USVs are bounded; therefore, Assumption 1 is reasonable.

Assumption 2. The velocity of the i th USV is bounded such that $\|v_i\| \leq v_i^*$, v_i^* is a positive constant.

The control inputs to drive USVs are bounded, and the energy of external disturbances is limited. Therefore, Assumption 2 is reasonable.

Assumption 3. The desired distance ($\rho_{ij,d}$) and angle ($\lambda_{ij,d}$) are bounded.

Assumption 3 means that the desired value is reasonable.

The following definitions are posited.

As shown in Figure 2, the subscript j is the index of the leader (j). $\eta_j = [x_j, y_j, \psi_j]^T$ is used to denote the position and yaw of the leader (j). $v_j = [u_j, v_j, r_j]^T$ is the velocity and yaw rate of the leader (j).

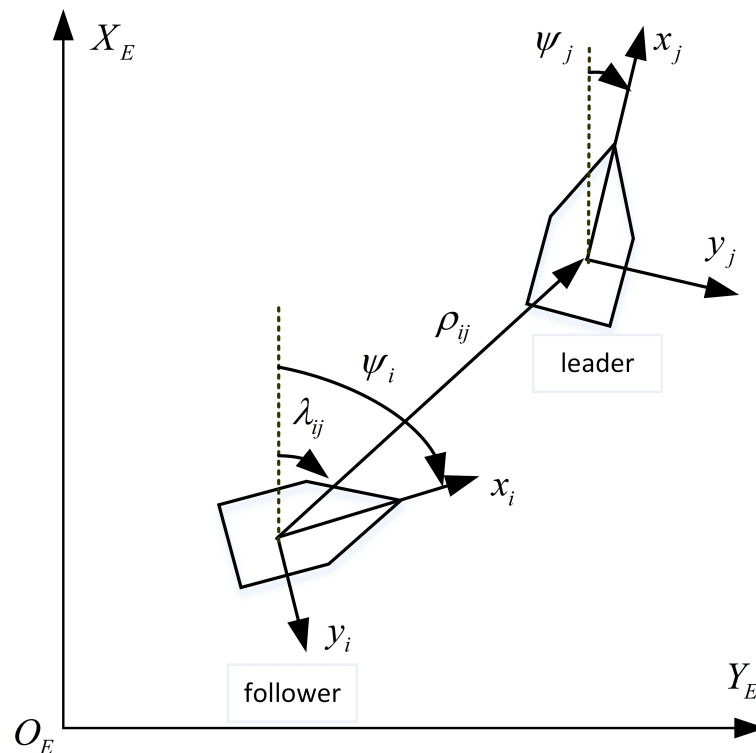


Figure 2. Leader–follower structure.

The relative distance (ρ_{ij}) and angle (λ_{ij}) between the i th USV and the leader (j) are expressed as

$$\rho_{ij} = \sqrt{(x_j - x_i)^2 + (y_j - y_i)^2}, \tag{9}$$

$$\lambda_{ij} = \text{atan2}(y_j - y_i, x_j - x_i). \tag{10}$$

The differential equations of ρ_{ij} and λ_{ij} are given by:

$$\begin{aligned} \dot{\rho}_{ij} &= \frac{(x_j - x_i)(\dot{x}_j - \dot{x}_i) + (y_j - y_i)(\dot{y}_j - \dot{y}_i)}{\sqrt{(x_j - x_i)^2 + (y_j - y_i)^2}} \\ &= \frac{(x_j - x_i)(\dot{x}_j - \dot{x}_i) + (y_j - y_i)(\dot{y}_j - \dot{y}_i)}{\rho_{ij}}, \end{aligned} \tag{11}$$

$$\dot{\lambda}_{ij} = \frac{1}{1 + \frac{(y_j - y_i)^2}{(x_j - x_i)^2}} \frac{(\dot{y}_j - \dot{y}_i)(x_j - x_i) - (\dot{x}_j - \dot{x}_i)(y_j - y_i)}{(x_j - x_i)^2}. \tag{12}$$

According to $x_j - x_i = \rho_{ij} \cos(\lambda_{ij})$ and $y_j - y_i = \rho_{ij} \sin(\lambda_{ij})$,

$$\begin{aligned} \dot{\rho}_{ij} &= [u_j \cos(\psi_j) - v_j \sin(\psi_j) - u_i \cos(\psi_i) + v_i \sin(\psi_i)] \cos(\lambda_{ij}) \\ &\quad + [u_j \sin(\psi_j) + v_j \cos(\psi_j) - u_i \sin(\psi_i) + v_i \cos(\psi_i)] \sin(\lambda_{ij}) \\ &= -u_i \cos(\psi_i - \lambda_{ij}) + u_j \cos(\psi_j - \lambda_{ij}) \\ &\quad + v_i \sin(\psi_i - \lambda_{ij}) - v_j \sin(\psi_j - \lambda_{ij}) \end{aligned} \tag{13}$$

$$\begin{aligned} \dot{\lambda}_{ij} &= \frac{(\dot{y}_j - \dot{y}_i)\rho_{ij} \cos(\lambda_{ij}) - (\dot{x}_j - \dot{x}_i)\rho_{ij} \sin(\lambda_{ij})}{\rho_{ij}^2} \\ &= \frac{1}{\rho_{ij}} \{-u_i \sin(\psi_i - \lambda_{ij}) + u_j \sin(\psi_j - \lambda_{ij}) \\ &\quad - v_i \cos(\psi_i - \lambda_{ij}) + v_j \cos(\psi_j - \lambda_{ij})\}. \end{aligned} \tag{14}$$

The control objective is to design an event-triggered control law for USVs to track the leader with a desired distance ($\rho_{ij,d}$) and angle ($\lambda_{ij,d}$).

Remark 1. In the controller design process, the i th USV tracks the j th USV using the x_j , y_j and ψ_j information. This means that communication costs are not saved between multiple USVs.

3. Event-Triggered Extended-State Observer

An ETESO was developed to estimate uncertainties including model uncertainties and time-varying disturbances, and an event-triggered condition was employed to avoid unnecessary communications. Inspired by [33], an ETESO was designed as follows:

$$\dot{\hat{\eta}}_i(t) = -\frac{3}{\epsilon_i}(\hat{\eta}_i - \xi_i) + R_i \hat{v}_i, \tag{15}$$

$$\dot{\hat{v}}_i(t) = -\frac{3}{\epsilon_i^2} R_i^T (\hat{\eta}_i - \xi_i) + \hat{\sigma}_i + M_i^{-1} \tau_i, \tag{16}$$

$$\dot{\hat{\sigma}}_i(t) = -\frac{1}{\epsilon_i^3} R_i^T (\hat{\eta}_i - \xi_i), \tag{17}$$

where $\hat{\eta}_i = [\hat{x}_i, \hat{y}_i, \hat{\psi}_i]^T$; $\hat{v}_i = [\hat{u}_i, \hat{v}_i, \hat{r}_i]^T$; and $\hat{\sigma}_i = [\hat{\sigma}_{i,1}, \hat{\sigma}_{i,2}, \hat{\sigma}_{i,3}]^T$; $\hat{x}_i, \hat{y}_i, \hat{\psi}_i, \hat{u}_i, \hat{v}_i, \hat{r}_i, \hat{\sigma}_{i,1}, \hat{\sigma}_{i,2}$ and $\hat{\sigma}_{i,3}$ are the estimates of $x_i, y_i, \psi_i, u_i, v_i, r_i, \sigma_{i,1}, \sigma_{i,2}$ and $\sigma_{i,3}$, respectively; ϵ_i is a positive constant; and ζ_i is the transmitted signal given by

$$\zeta_i(t) = \begin{cases} \eta_i(t_k), & \text{if } d(t) = 0 \\ \eta_i(t), & \text{otherwise;} \end{cases} \tag{18}$$

t_k is the previous event-triggering time instant; $d(t)$ is an event-triggered mechanism designed as

$$d(t) = \begin{cases} 0, & \text{if } \|q(t)\| < c_q \\ 1, & \text{otherwise.} \end{cases} \tag{19}$$

$c_q > 0$ is the design threshold; and

$$q(t) = [q_1, q_2, q_3]^T = [\eta_i(t_k) - \eta_i(t)] / \epsilon_i^2. \tag{20}$$

Remark 2. The continuous-time control scheme is emulated by a computer with a sampler and a zero-order holder, and the control command is updated periodically. At each sampling instant, $q(t)$ is monitored to determine whether or not to transmit the information ($\eta_i(t)$) to the observer. If $\|q(t)\| \geq c_q$, the event-triggering time instant (t_k) is updated to the current time (t), and $\eta_i(t)$ is transmitted to the observer. Otherwise, only $\eta_i(t_k)$ is available to the observer. The first event-triggering time is $t_1 = 0$.

To facilitate controller design and stability analysis, $\zeta_i = [\zeta_{i,1}, \zeta_{i,2}, \zeta_{i,3}]^T$ (16) can be written as

$$\dot{u}_i = \zeta_{i,1} + \hat{\sigma}_{i,1} + \frac{\tau_{i,uc} - \omega_{i,u}}{m_{i,11}}, \tag{21}$$

$$\dot{v}_i = \zeta_{i,2} + \hat{\sigma}_{i,2}, \tag{22}$$

$$\dot{r}_i = \zeta_{i,3} + \hat{\sigma}_{i,3} + \frac{\tau_{i,rc} - \omega_{i,r}}{m_{i,33}} \tag{23}$$

with

$$\zeta_{i,1} = -\frac{3}{\epsilon_i^2} [\cos(\psi_i)(\hat{x}_i - \zeta_{i,1}) + \sin(\psi_i)(\hat{y}_i - \zeta_{i,2})], \tag{24}$$

$$\zeta_{i,2} = -\frac{3}{\epsilon_i^2} [-\sin(\psi_i)(\hat{x}_i - \zeta_{i,1}) + \cos(\psi_i)(\hat{y}_i - \zeta_{i,2})], \tag{25}$$

$$\zeta_{i,3} = -\frac{3}{\epsilon_i^2} (\hat{\psi}_i - \zeta_{i,3}), \tag{26}$$

Define $\tilde{x}_i = \hat{x}_i - x_i, \tilde{y}_i = \hat{y}_i - y_i, \tilde{\psi}_i = \hat{\psi}_i - \psi_i, \tilde{u}_i = \hat{u}_i - u_i, \tilde{v}_i = \hat{v}_i - v_i, \tilde{r}_i = \hat{r}_i - r_i,$

$$\tilde{\eta}_i = [\tilde{x}_i, \tilde{y}_i, \tilde{\psi}_i]^T, e_{i,1}(t) = [e_{11}, e_{12}, e_{13}]^T = \frac{\tilde{\eta}_i(\epsilon_i t)}{\epsilon_i^2}, \tag{27}$$

$$\tilde{v}_i = [\tilde{u}_i, \tilde{v}_i, \tilde{r}_i]^T, e_{i,2}(t) = \frac{\tilde{v}_i(\epsilon_i t)}{\epsilon_i}, \tag{28}$$

$$\tilde{\sigma}_i = \hat{\sigma}_i - \sigma_i, e_{i,3}(t) = \tilde{\sigma}_i(\epsilon_i t). \tag{29}$$

It follows that

$$\dot{e}_{i,1}(t) = -3e_{i,1}(t) - 3q(t) + R_i(\psi_i(t))e_{i,2}(t), \tag{30}$$

$$\begin{aligned} \dot{e}_{i,2}(t) = & -3R_i^T(\psi_i(t))e_{i,1}(t) - 3R_i^T(\psi_i(t))q(t) \\ & + e_{i,3}(t), \end{aligned} \tag{31}$$

$$\dot{e}_{i,3}(t) = -R_i^T(\psi_i(t))e_{i,1}(t) - R_i^T(\psi_i(t))q(t) - \epsilon_i \dot{\sigma}_i. \tag{32}$$

Theorem 1. Consider the USV models (7) and (8), the ETESO (15)–(17) and the event-triggering condition (19). If Assumptions 1 and 2 are satisfied, there exist $\epsilon_i > 0$ and $\iota > 0$ such that for any $k > 0$,

$$\min\{t_{k+1} - t_k\} \geq \iota. \tag{33}$$

Proof. Along with (18) and (19), the event-triggering mechanism can be described as

$$\tilde{\zeta}_i(t) = \begin{cases} \eta_i(t_k), & \text{if } \|\eta_i(t_k) - \eta_i(t)\| < c_q \epsilon_i^2 \\ \eta_i(t), & \text{otherwise.} \end{cases} \tag{34}$$

When $t \in [t_k, t_{k+1})$, the sample error $(\eta_i(t_k) - \eta_i(t))$ becomes

$$\begin{aligned} \|\eta_i(t_k) - \eta_i(t)\| &= \left\| \int_{t_k}^t \dot{\eta}_i(\iota) d\iota \right\| \\ &\leq \int_{t_k}^t \|R_i(\psi_i(\iota))v_i\| d\iota. \end{aligned} \tag{35}$$

Assumption 2 implies that

$$\|\eta_i(t_k) - \eta_i(t)\| \leq (t - t_k)v_i^*. \tag{36}$$

There exist $\iota = \epsilon_i^2 c_q / v^*$ and $\iota = t - t_k$ such that $\|\eta_i(t_k) - \eta_i(t)\| \leq c_q \epsilon_i^2$. It is worth noting that $t \in [t_k, t_{k+1})$, leading to the conclusion that $\min\{t_{k+1} - t_k\} \geq \iota$.

Theorem 1 shows that Zeno behavior can be avoided by using the proposed observer. Next, the error dynamics of the proposed ETESO are investigated.

To facilitate stability analysis, the following definitions are posited: $E_i(t) = [e_{i,1}(t)^T, e_{i,2}(t)^T, e_{i,3}(t)^T]^T \in \mathbb{R}^9$. The error dynamics (Equations (30)–(32)) can be expressed as

$$\dot{E}_i(t) = A_i E_i(t) - B_i \epsilon_i \dot{\sigma}_i(t) - H_i D_i q(t), \tag{37}$$

$$A_i = \begin{bmatrix} -3I_3 & R_i(\psi_i(t)) & 0_3 \\ -3R_i^T(\psi_i(t)) & 0_3 & I_3 \\ -R_i^T(\psi_i(t)) & 0_3 & 0_3 \end{bmatrix}, \tag{38}$$

$$B_i = \begin{bmatrix} 0_3 \\ 0_3 \\ I_3 \end{bmatrix}, \tag{39}$$

$$D_i = \begin{bmatrix} 3_3 \\ 3_3 \\ I_3 \end{bmatrix}, \tag{40}$$

and $H_i = \text{diag}\{I_3, R_i^T(\psi_i(t)), R_i^T(\psi_i(t))\}$.

Using a transformation ($E_t(t) = T E_i(t)$, where $T = \text{diag}\{R_i^T(\psi_i(t)), I_3, I_3\}$), it follows that

$$\dot{E}_t(t) = A_0 E_t(t) + r_i S_T E_t(t) - B_i \epsilon_i \dot{\sigma}_i(t) - \bar{H}_i D_i q(t), \tag{41}$$

where $\bar{H}_i = \text{diag}\{R^T(\psi_i(t)), R^T(\psi_i(t)), R^T(\psi_i(t))\}$, $S_T = \text{diag}\{S^T, 0_3, 0_3\}$, and

$$A_0 = \begin{bmatrix} -3I_3 & I_3 & 0_3 \\ -3I_3 & 0_3 & I_3 \\ -I_3 & 0_3 & 0_3 \end{bmatrix}, \tag{42}$$

$$S = \begin{bmatrix} 0 & -1 & 0 \\ 1 & 0 & 0 \\ 0 & 0 & 0 \end{bmatrix}. \tag{43}$$

□

Theorem 2. *The observer error dynamics are bounded if there exists a positive definite matrix (P) satisfying the inequalities used in stability analysis, and the inequalities are defined as*

$$A_0^T P + PA_0 + \rho I_9 - \bar{r}_i(S_T^T P + PS_T) \leq 0, \tag{44}$$

$$A_0^T P + PA_0 + \rho I_9 + \bar{r}_i(S_T^T P + PS_T) \leq 0, \tag{45}$$

where ρ is a positive constant, and \bar{r}_i is the upper bound of r_i .

Proof. Consider the Lyapunov function:

$$V_o = \frac{1}{2} E_t(t)^T P E_t(t). \tag{46}$$

Differentiating V_o with respect to time

$$\begin{aligned} \dot{V}_o &= \frac{1}{2} E_t(t)^T (A_0^T P + r_i S_T^T P + PA_0 + r_i PS_T) E_t(t) \\ &\quad - E_t(t)^T P B_i \epsilon_i \dot{\sigma}_i(t) - E_t(t)^T P \bar{H}_i D_i q(t) \\ &\leq -\frac{\rho}{2} \|E_t(t)\|^2 + \epsilon_i \|E_t(t)\| \|PB_i\| \|\dot{\sigma}_i(t)\| \\ &\quad + \|E_t(t)\| \|PD_i\| \|q(t)\|. \end{aligned} \tag{47}$$

It is worth noting that $2\epsilon_i \|PB_i\| \|\dot{\sigma}_i(t)\| + 2\|PD_i\| \|q(t)\| \leq \rho c_{o1} \|E_t(t)\|$, $0 < c_{o1} < 1$, leading to

$$\dot{V}_o \leq -\frac{\rho}{2} (1 - c_{o1}) \|E_t(t)\|^2 \leq -c_{o2} V_o, \tag{48}$$

where $c_{o2} = \rho(1 - c_{o1}) / \lambda_{\max}(P)$.

Then, the state $E_t(t)$ is bounded. Given that $\|T^{-1}\| = 1$ and $E_i(t) = T^{-1} E_t(t)$, the estimation error ($E_i(t)$) is bounded. □

4. Controller Design

An output feedback controller combined with the ETESO was developed based on an event-triggered strategy. As shown in Figure 3, the characteristic of the proposed controller are as follows. The estimator is used to estimate the velocity of the leader. The ETESO was designed to provide the velocity, yaw rate and uncertainties. The transmitted signal contains an event-triggered strategy that reduces sensor-to-observer communication costs. The triggering condition of the controller can largely reduce the action times of the actuators. The control law design process is divided into the following steps.

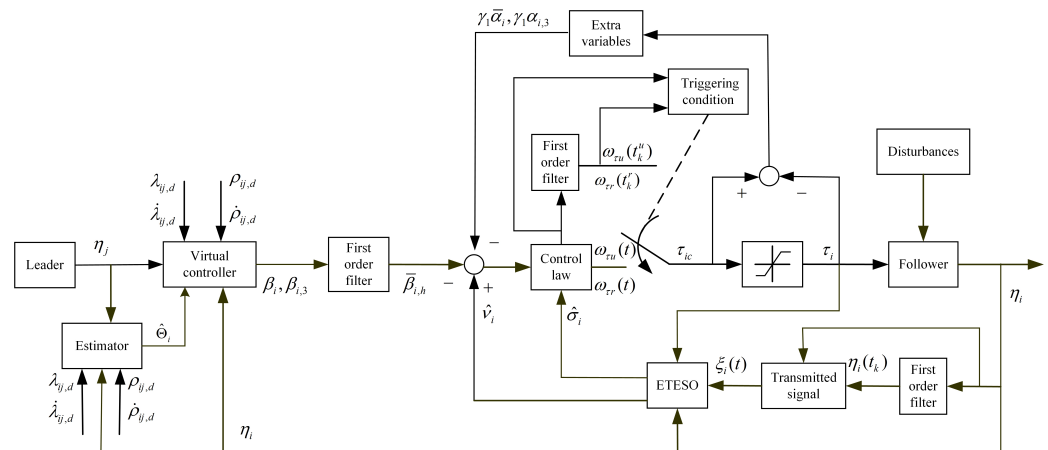


Figure 3. Structure of the proposed ETC.

Step 1: Define the formation tracking error vector:

$$P_{ij} = [\rho_{ij,e}, \lambda_{ij,e}]^T, \tag{49}$$

where $\rho_{ij,e} = \rho_{ij} - \rho_{ij,d}$, and $\lambda_{ij,e} = \lambda_{ij} - \lambda_{ij,d}$.

Using (13) and (14), the time derivative of P_{ij} is given as

$$\dot{P}_{ij} = B_{ij}(-\Xi_{ij,1}z_i + \Xi_{ij,2}z_j - D_{ij,d}), \tag{50}$$

where $B_{ij} = \text{diag}\{1, \frac{1}{\rho_{ij}}\}$,

$$\Xi_{ij,1} = \begin{bmatrix} \cos(\psi_i - \lambda_{ij}) & -\sin(\psi_i - \lambda_{ij}) \\ \sin(\psi_i - \lambda_{ij}) & \cos(\psi_i - \lambda_{ij}) \end{bmatrix}, \tag{51}$$

$$\Xi_{ij,2} = \begin{bmatrix} \cos(\psi_j - \lambda_{ij}) & -\sin(\psi_j - \lambda_{ij}) \\ \sin(\psi_j - \lambda_{ij}) & \cos(\psi_j - \lambda_{ij}) \end{bmatrix}, \tag{52}$$

$z_i = [u_i, v_i]^T$, $z_j = [u_j, v_j]^T$ and $D_{ij,d} = [\dot{\rho}_{ij,d}, \dot{\lambda}_{ij,d}]^T$.

Additionally, $f_i = [f_{i,1} \ f_{i,2}] = P_{ij}^T B_{ij} \Xi_{ij,1}$, and $\|f_i\| \leq f_i^*$, f_i^* is an unknown positive constant.

Remark 3. The definitions of $\Xi_{ij,1}$, P_{ij} and B_{ij} , indicate that $\|\Xi_{ij,1}\| = 1$, P_{ij} and B_{ij} are bounded, so $\|f_i\| \leq f_i^*$ is reasonable.

Choosing β_i as a virtual controller, β_i is designed as:

$$\beta_i = \bar{\Xi}_{ij,1}^{-1} (B_{ij}^{-1} K_{i,1} P_{ij} + \hat{\Theta}_i - D_{ij,d}) + \bar{f}_{i,2} \tag{53}$$

where $\bar{\Xi}_{ij,1}^{-1} = \Xi_{ij,1}^T (\Xi_{ij,1} \Xi_{ij,1}^T)^{-1}$, $K_{i,1} \in \mathbb{R}^{2 \times 2}$ is a positive definite matrix, $\bar{f}_{i,2} = [0, \tanh(f_{i,2}/\epsilon_f)]^T$, $\epsilon_f > 0$ is a constant, $\hat{\Theta}_i$ is the estimator of Θ_i , $\Theta_i = \Xi_{ij,2}z_j$ and it updated as

$$\dot{\hat{\Theta}}_i = -K_{\Theta} \hat{\Theta}_i - \bar{P}_{ij}, \tag{54}$$

where $\bar{P}_{ij} = B_{ij} [\rho_{ij,e} \tanh(\rho_{ij,e}/\epsilon_\rho), \lambda_{ij,e} \tanh(\lambda_{ij,e}/\epsilon_\lambda)]^T$, K_{Θ} is a positive definite matrix, and ϵ_ρ and ϵ_λ are positive constants.

Remark 4. The adaptive term $\hat{\Theta}_i$ is employed to reduce the volume of data contained in the formation communication [32] and estimate the information (Θ_i). Θ_i can be estimated because $\Xi_{ij,2}z_j \leq |z_j|$, and z_j is bounded, ensuring that formation tracking control is achieved without velocity of the leader and that the amount of data exchanged between USVs can be reduced. Unlike

the controller presented in [32], the proposed controller was designed without the velocities of follower. The ETESO can reduce sensor-to-observer communication costs, and the ETC can largely reduce the action times of actuators.

Step 2: An error is defined as

$$\psi_{i,e} = \psi_i - \psi_{ij,a}, \tag{55}$$

where

$$\psi_{ij,a} = [\arctan2(g_{ij,1}, g_{ij,2}) - \psi_j] \tanh(g_{ij,3}) + \psi_j, \tag{56}$$

where

$$g_{ij,1} = \rho_{ij} \sin(\lambda_{ij}) - \rho_{ij,d} \sin(\lambda_{ij,d}), \tag{57}$$

$$g_{ij,2} = \rho_{ij} \cos(\lambda_{ij}) - \rho_{ij,d} \cos(\lambda_{ij,d}), \tag{58}$$

$$g_{ij,3} = \{(\rho_{ij,d} - \rho_{ij})^2 + (\lambda_{ij,d} - \lambda_{ij})^2\} / \gamma_{ij}, \tag{59}$$

where γ_{ij} is a positive constant.

According to USV dynamics, the time derivative of $\psi_{i,e}$ is

$$\dot{\psi}_{i,e} = r_i - \dot{\psi}_{ij,a}. \tag{60}$$

The virtual control $\beta_{i,3}$ is chosen as:

$$\beta_{i,3} = -k_{i,2}\psi_{i,e} + \dot{\psi}_{ij,a}, \tag{61}$$

where $k_{i,2}$ is a positive constant.

Step 3: Error functions are defined as follows:

$$z_{i,e} = [u_{i,e}, v_{i,e}]^T = \hat{z}_i - \bar{\beta}_i - \gamma_1 \bar{\alpha}_i, \tag{62}$$

$$r_{i,e} = \hat{r}_i - \bar{\beta}_{i,3} - \gamma_1 \alpha_{i,3}, \tag{63}$$

$$\omega_i = \bar{\beta}_i - \beta_i, \tag{64}$$

$$\omega_{i,3} = \bar{\beta}_{i,3} - \beta_{i,3}, \tag{65}$$

where $\hat{z}_i = [\hat{u}_i, \hat{v}_i]^T$; $\bar{\beta}_i = [\bar{\beta}_{i,1}, \bar{\beta}_{i,2}]^T$; γ_1 is a positive constant; $\bar{\beta}_{i,h}$, $h = 1, 2, 3$, is derived from the first-order filter $l_{i,h}\dot{\bar{\beta}}_{i,h} + \bar{\beta}_{i,h} = \beta_{i,h}$; $l_{i,h} > 0$ is a constant; $\bar{\alpha}_i = [\alpha_{i,1}, \tanh(\alpha_{i,2})/\gamma_1]^T$ $\alpha_{i,h}$, $h = 1, 2, 3$, is the auxiliary variable derived to deal with the underactuated problem and input saturation. $\omega_i = [\omega_{i,1}, \omega_{i,2}]^T$, $\omega_{i,h}$, $h = 1, 2, 3$, is the error caused by the first order filter.

The updated laws of extra variables are given by

$$\dot{\alpha}_{i,1} = \frac{1}{\gamma_1} (-T_u \alpha_{i,1} - \frac{\omega_{i,u}}{m_{i,11}}), \tag{66}$$

$$\dot{\alpha}_{i,2} = \frac{1}{\cosh^2(\alpha_{i,2})} (\hat{\sigma}_{i,2} + k_{i,4} v_{i,e} - f_{i,2} - \dot{\bar{\beta}}_{i,2}), \tag{67}$$

$$\dot{\alpha}_{i,3} = \frac{1}{\gamma_1} (-T_r \alpha_{i,3} - \frac{\omega_{i,r}}{m_{i,33}}), \tag{68}$$

where T_u , $k_{i,4}$ and T_r are positive constants.

Step 4: A control law at the kinetic level is designed as

$$\omega_{\tau u}(t) = m_{i,11} (-k_{i,3} u_{i,e} + \dot{\bar{\beta}}_{i,1} - T_u \alpha_{i,1} + f_{i,1} - \hat{\sigma}_{i,1}), \tag{69}$$

$$\omega_{\tau r}(t) = m_{i,33} (-k_{i,5} r_{i,e} + \dot{\bar{\beta}}_{i,3} - T_r \alpha_{i,3} - \psi_{i,e} - \hat{\sigma}_{i,3}), \tag{70}$$

where $k_{i,3}$ and $k_{i,5}$ are positive constants.

Remark 5. In the common continuous control schemes, the controller design has already been completed in Step 4. Here, an event-triggered controller is designed, and the event-triggered condition is established in the following step. During the flow period between two successive triggering instants, a zero-order holder is used to keep input signals unchanged. The key to a successful ETC design is to choose an appropriate event-triggered strategy. In [23], the triggered condition of a time-varying threshold event-triggered controller (TTETC) is constructed based on flow time and the Lyapunov function. Therefore, the action times of the actuators are limited, and Zeno behavior can be avoided. The signals calculated by controller should be closely related to the triggered condition, its size change determines whether or not to update the control inputs and the change is used to design the proposed triggered condition. It is necessary to provide proof that Zeno behavior is avoided. The appropriate event-triggered strategy reduces the action times of the actuators.

An event-triggered controller is chosen as

$$\begin{cases} \tau_{i,uc}(t) = \omega_{\tau u}(t_k^u), & \forall t \in [t_k^u, t_{k+1}^u) \\ \tau_{i,rc}(t) = \omega_{\tau r}(t_k^r), & \forall t \in [t_k^r, t_{k+1}^r) \end{cases} \quad (71)$$

where

$$\begin{cases} t_k^u = \inf\{t \in \mathbb{R} \mid |e_u(t)| \geq a_1\}, & t_1^u = 0 \\ t_k^r = \inf\{t \in \mathbb{R} \mid |e_r(t)| \geq a_2\}, & t_1^r = 0 \\ e_u = \omega_{\tau u} - \tau_{i,uc}, \quad e_r = \omega_{\tau r} - \tau_{i,rc}, \end{cases} \quad (72)$$

and a_1 and a_2 are positive constants.

The following theorem is provided to demonstrate the stability of the overall closed-loop system.

Theorem 3. Consider a system consisting of USV dynamics ((7) and (8)), an observer ((15)–(17)), auxiliary variables ((66)–(68)), a control law (71) and environmental disturbances under Assumptions 1–3. Then, the proposed control scheme guarantees that (1) all signals in the closed-loop system are bounded and (2) all USVs can track the leader with a bounded tracking error.

Proof. Choose a Lyapunov function candidate as follows:

$$\begin{aligned} V_1 = & \frac{1}{2} P_{ij}^T P_{ij} + \frac{1}{2} \psi_{i,e}^2 + \frac{1}{2} u_{i,e}^2 + \frac{1}{2} v_{i,e}^2 + \frac{1}{2} r_{i,e}^2 \\ & + \frac{1}{2} \tilde{\Theta}_i^T \tilde{\Theta}_i + \frac{1}{2} \sum_{h=1}^3 \omega_{i,h}^2 + \frac{1}{2} \alpha_{i,1}^2 + \frac{1}{2} \alpha_{i,3}^2, \end{aligned} \quad (73)$$

where $\tilde{\Theta}_i = \hat{\Theta}_i - \Theta_i$.

Along with (50) and (60), the time derivative of V_1 is expressed as

$$\begin{aligned} \dot{V}_1 = & P_{ij}^T B_i (-\Xi_{ij,1} z_i + \Xi_{ij,2} z_j - D_{ij,d}) + \psi_{i,e} (r_i - \dot{\psi}_{i,d}) \\ & + u_{i,e} (\dot{u}_i - \dot{\beta}_{i,1} - \gamma_1 \dot{\alpha}_{i,1}) + v_{i,e} (\dot{v}_i - \dot{\beta}_{i,2} - \dot{\alpha}_{i,2}) \\ & + r_{i,e} (\dot{r}_i - \dot{\beta}_{i,3} - \gamma_1 \dot{\alpha}_{i,3}) + \tilde{\Theta}_i^T \dot{\tilde{\Theta}}_i + \sum_{h=1}^3 \omega_{i,h} \dot{\omega}_{i,h} \\ & + \alpha_{i,1} \dot{\alpha}_{i,1} + \alpha_{i,3} \dot{\alpha}_{i,3}. \end{aligned} \quad (74)$$

By applying (21)–(23), (62) and (63) to (74), we obtain

$$\begin{aligned} \dot{V}_1 = & P_{ij}^T B_i [-\Xi_{ij,1}(z_{i,e} + \beta_i + \omega_i + \gamma_1 \bar{\alpha}_i - \bar{z}_i) + \Xi_{ij,2} z_j \\ & - D_{ij,d}] + \psi_{i,e}(r_{i,e} + \beta_{i,3} + \omega_{i,3} + \gamma_1 \alpha_{i,3} - \tilde{r}_i \\ & - \psi_{i,a}) + u_{i,e}(\zeta_{i,1} + \hat{\sigma}_{i,1} + \frac{\tau_{i,uc} - \omega_{i,u}}{m_{i,11}} - \dot{\beta}_{i,1} \\ & - \gamma_1 \dot{\alpha}_{i,1}) + v_{i,e}(\zeta_{i,2} + \hat{\sigma}_{i,2} - \dot{\beta}_{i,2} - \dot{\alpha}_{i,2}) \\ & + r_{i,e}(\zeta_{i,3} + \hat{\sigma}_{i,3} + \frac{\tau_{i,rc} - \omega_{i,r}}{m_{i,33}} - \dot{\beta}_{i,3} - \gamma_1 \dot{\alpha}_{i,3}) \\ & - \tilde{\Theta}_i^T K_{\Theta} \hat{\Theta}_i - \tilde{\Theta}_i^T \bar{P}_{ij} + \sum_{h=1}^3 \omega_{i,h} \dot{\omega}_{i,h} + \alpha_{i,1} \dot{\alpha}_{i,1} \\ & + \alpha_{i,3} \dot{\alpha}_{i,3}. \end{aligned} \tag{75}$$

Using (53), (54), (61) and (66)–(68) yields

$$\begin{aligned} \dot{V}_1 = & -P_{ij}^T K_{i,1} P_{ij} - k_{i,2} \psi_{i,e}^2 - P_{ij}^T B_{ij} \tilde{\Theta}_i \\ & - f_i(z_{i,e} + \omega_i + \gamma_1 \bar{\alpha}_i + \bar{f}_{i,2} - \bar{z}_i) \\ & + \psi_{i,e}(r_{i,e} + \omega_{i,3} + \gamma_1 \alpha_{i,3} - \tilde{r}_i) \\ & + u_{i,e}(\zeta_{i,1} + \hat{\sigma}_{i,1} + \frac{\tau_{i,uc}}{m_{i,11}} - \dot{\beta}_{i,1} + T_u \alpha_{i,1}) \\ & + v_{i,e}(-k_{i,4} v_{i,e} + \zeta_{i,2} + f_{i,2}) \\ & + r_{i,e}(\zeta_{i,3} + \hat{\sigma}_{i,3} + \frac{\tau_{i,rc}}{m_{i,33}} - \dot{\beta}_{i,3} + T_r \alpha_{i,3}) \\ & - \tilde{\Theta}_i^T K_{\Theta} \hat{\Theta}_i - \tilde{\Theta}_i^T \bar{P}_{ij} - \sum_{h=1}^3 \omega_{i,h} (\frac{\omega_{i,h}}{l_{i,h}} + \dot{\beta}_{i,h}) \\ & - \bar{T}_u \alpha_{i,1}^2 - \alpha_{i,1} \bar{\omega}_{i,u} - \bar{T}_r \alpha_{i,3}^2 - \alpha_{i,3} \bar{\omega}_{i,r}, \end{aligned} \tag{76}$$

where $\bar{T}_u = T_u / \gamma_1$, $\bar{\omega}_{i,u} = \omega_{i,u} / m_{i,11}$, $\bar{T}_r = T_r / \gamma_1$ and $\bar{\omega}_{i,r} = \omega_{i,r} / m_{i,33}$.

According to (71) and (72), $|\omega_{\tau u} - \tau_{i,uc}| \leq a_1$ and $|\omega_{\tau r} - \tau_{i,rc}| \leq a_2$. There exist time-varying functions (μ_1, μ_2) satisfying $|\mu_1| \leq 1$ and $|\mu_2| \leq 1$. Then, $\omega_{\tau u} = \tau_{i,uc} + \mu_1 a_1$ and $\omega_{\tau r} = \tau_{i,rc} + \mu_2 a_2$.

It is worth noting that $f_i z_{i,e} = f_{i,1} u_{i,e} + f_{i,2} v_{i,e}$, and

$$\begin{aligned} -P_{ij}^T B_{ij} \tilde{\Theta}_i - \tilde{\Theta}_i^T \bar{P}_{ij} & \leq |P_{ij}^T B_{ij} \tilde{\Theta}_i| - \tilde{\Theta}_i^T \bar{P}_{ij} \\ & \leq 0.2758 \epsilon_{\rho} + 0.2758 \epsilon_{\lambda}. \end{aligned} \tag{77}$$

Along with (69) and (70), \dot{V}_1 becomes

$$\begin{aligned} \dot{V}_1 \leq & -P_{ij}^T K_{i,1} P_{ij} - k_{i,2} \psi_{i,e}^2 - k_{i,3} u_{i,e}^2 - k_{i,4} v_{i,e}^2 \\ & - k_{i,5} r_{i,e}^2 - \bar{T}_u \alpha_{i,1}^2 - \bar{T}_r \alpha_{i,3}^2 - f_i(\omega_i + \gamma_1 \bar{\alpha}_i \\ & + \bar{f}_{i,2} - \bar{z}_i) + \psi_{i,e}(\omega_{i,3} + \gamma_1 \alpha_{i,3} - \tilde{r}_i) \\ & + u_{i,e}(\zeta_{i,1} - \frac{\mu_1 a_1}{m_{i,11}}) + v_{i,e} \zeta_{i,2} + r_{i,e}(\zeta_{i,3} - \frac{\mu_2 a_2}{m_{i,33}}) \\ & - \tilde{\Theta}_i^T K_{\Theta} \hat{\Theta}_i + 0.2758 \epsilon_{\rho} + 0.2758 \epsilon_{\lambda} \\ & - \sum_{h=1}^3 \omega_{i,h} (\frac{\omega_{i,h}}{l_{i,h}} + \dot{\beta}_{i,h}) - \alpha_{i,1} \bar{\omega}_{i,u} - \alpha_{i,3} \bar{\omega}_{i,r}. \end{aligned} \tag{78}$$

According to Young’s inequality,

$$\begin{aligned}
 -\tilde{\Theta}_i^T K_{\Theta} \hat{\Theta}_i &\leq -k_{\Theta} \tilde{\Theta}_i^T (\tilde{\Theta}_i + \Theta_i) \\
 &\leq \frac{k_{\Theta}}{2} (-\tilde{\Theta}_i^T \tilde{\Theta}_i + \Theta_i^T \Theta_i)
 \end{aligned}
 \tag{79}$$

where $k_{\Theta} = \lambda_{\min}(K_{\Theta})$.
 \dot{V}_1 becomes

$$\begin{aligned}
 \dot{V}_1 &\leq -P_{ij}^T K_{i,1} P_{ij} - k_{i,2} \psi_{i,e}^2 - k_{i,3} u_{i,e}^2 - k_{i,4} v_{i,e}^2 \\
 &\quad - k_{i,5} r_{i,e}^2 - \bar{T}_u \alpha_{i,1}^2 - \bar{T}_r \alpha_{i,3}^2 - \frac{k_{\Theta}}{2} \tilde{\Theta}_i^T \tilde{\Theta}_i \\
 &\quad - f_i(\omega_i + \gamma_1 \bar{\alpha}_i + \bar{f}_{i,2} - \bar{z}_i) \\
 &\quad + \psi_{i,e}(\omega_{i,3} + \gamma_1 \alpha_{i,3} - \bar{r}_i) + u_{i,e}(\zeta_{i,1} - \frac{\mu_1 a_1}{m_{i,11}}) \\
 &\quad + v_{i,e} \zeta_{i,2} + r_{i,e}(\zeta_{i,3} - \frac{\mu_2 a_2}{m_{i,33}}) \\
 &\quad - \sum_{h=1}^3 \omega_{i,h} (\frac{\omega_{i,h}}{l_{i,h}} + \dot{\beta}_{i,h}) - \alpha_{i,1} \bar{\omega}_{i,u} - \alpha_{i,3} \bar{\omega}_{i,r} \\
 &\quad + \frac{k_{\Theta}}{2} \Theta_i^T \Theta_i + 0.2758 \epsilon_{\rho} + 0.2758 \epsilon_{\lambda}.
 \end{aligned}
 \tag{80}$$

According to [36] and Young’s inequality,

$$\begin{aligned}
 -f_i(\gamma_1 \bar{\alpha}_{i,1} + \bar{f}_{i,2}) &= -\gamma_1 f_{i,1} \alpha_{i,1} - f_{i,2} \tanh(\alpha_{i,2}) \\
 &\quad - \tanh(f_{i,2} / \epsilon_f) \\
 &\leq \frac{\gamma_1^2}{2} f_{i,1}^2 + \frac{1}{2} \alpha_{i,1}^2 + 0.2785 \epsilon_f.
 \end{aligned}
 \tag{81}$$

The following inequalities are used for stability analysis:

$$\begin{aligned}
 f_i \bar{z}_i &= f_{i,1} \tilde{u}_i + f_{i,2} \tilde{v}_i \\
 &\leq \frac{1}{2} (f_{i,1}^2 + f_{i,2}^2 + \tilde{u}_i^2 + \tilde{v}_i^2) \\
 &\leq \frac{1}{2} (f_{i,1}^2 + f_{i,2}^2 + \epsilon_i^2 e_{11}^2 + \epsilon_i^2 e_{12}^2),
 \end{aligned}
 \tag{82}$$

$$\begin{aligned}
 \psi_{i,e}(\gamma_1 \alpha_{i,3} - \bar{r}_i) &\leq \frac{\gamma_1}{2} (\psi_{i,e}^2 + \alpha_{i,3}^2) + \frac{1}{2} \psi_{i,e}^2 + \frac{1}{2} \bar{r}_i^2 \\
 &\leq \frac{\gamma_1 + 1}{2} \psi_{i,e}^2 + \frac{\gamma_1}{2} \alpha_{i,3}^2 + \frac{1}{2} \epsilon_i^2 e_{13}^2,
 \end{aligned}
 \tag{83}$$

$$\begin{aligned}
 \zeta_{i,1} &\leq \frac{3}{\epsilon_i^2} (|\hat{x}_i - \bar{\zeta}_{i,1}| + |\hat{y}_i - \bar{\zeta}_{i,2}|) \\
 &\leq 3(|e_{11}| + |q_1| + |e_{12}| + |q_2|),
 \end{aligned}
 \tag{84}$$

$$\begin{aligned}
 \zeta_{i,2} &\leq \frac{3}{\epsilon_i^2} (|\hat{x}_i - \bar{\zeta}_{i,1}| + |\hat{y}_i - \bar{\zeta}_{i,2}|) \\
 &\leq 3(|e_{11}| + |q_1| + |e_{12}| + |q_2|),
 \end{aligned}
 \tag{85}$$

$$\zeta_{i,3} \leq \frac{3}{\epsilon_i^2} (|\hat{\psi}_i - \zeta_{i,3}|) \leq 3(|e_{13}| + |q_3|), \tag{86}$$

$$\begin{aligned} u_{i,e}(\zeta_{i,1} - \frac{\mu_1 a_1}{m_{i,11}}) &\leq u_{i,e}(\zeta_{i,1} + \bar{a}_1) \\ &\leq 3u_{i,e}(|e_{11}| + |q_1| + |e_{12}| + |q_2|) \\ &\quad + |u_{i,e}\bar{a}_1| \\ &\leq \frac{3}{2}(e_{11}^2 + q_1^2 + e_{12}^2 + q_2^2) + \frac{1}{2}\bar{a}_1 \\ &\quad + \frac{13}{2}u_{i,e}^2, \end{aligned} \tag{87}$$

$$\begin{aligned} v_{i,e}\zeta_{i,2} &\leq 3v_{i,e}(|e_{11}| + |q_1| + |e_{12}| + |q_2|) \\ &\leq \frac{3}{2}(e_{11}^2 + q_1^2 + e_{12}^2 + q_2^2) + 6v_{i,e}^2, \end{aligned} \tag{88}$$

$$\begin{aligned} r_{i,e}(\zeta_{i,3} - \frac{\mu_2 a_2}{m_{i,33}}) &\leq r_{i,e}(\zeta_{i,3} + \bar{a}_2) \\ &\leq 3r_{i,e}(|e_{13}| + |q_3|) + |r_{i,e}\bar{a}_2| \\ &\leq \frac{3}{2}(e_{13}^2 + q_3^2) + \frac{7}{2}r_{i,e}^2 + \frac{1}{2}\bar{a}_2^2, \end{aligned} \tag{89}$$

$$\alpha_{i,1}\bar{\omega}_{i,u} \leq \frac{1}{2}\alpha_{i,1}^2 + \frac{1}{2}\bar{\omega}_{i,u}^2 \tag{90}$$

$$\alpha_{i,3}\bar{\omega}_{i,r} \leq \frac{1}{2}\alpha_{i,3}^2 + \frac{1}{2}\bar{\omega}_{i,r}^2 \tag{91}$$

where $\bar{a}_1 = a_1/m_{i,11}$, and $\bar{a}_2 = a_2/m_{i,33}$.

Then, the following inequality can be obtained:

$$\begin{aligned} \dot{V}_1 &\leq -P_{ij}^T K_{i,1} P_{ij} - (k_{i,2} - \bar{\gamma}_1)\psi_{i,e}^2 - (k_{i,3} - \frac{13}{2})u_{i,e}^2 \\ &\quad - (k_{i,4} - 6)v_{i,e}^2 - (k_{i,5} - \frac{7}{2})r_{i,e}^2 - \frac{k_{\Theta}}{2}\bar{\Theta}_i^T \bar{\Theta}_i \\ &\quad - (\bar{T}_u - \frac{1}{2})\alpha_{i,1}^2 - (\bar{T}_r - \bar{\gamma}_1)\alpha_{i,3}^2 - f_i \omega_i \\ &\quad + \psi_{i,e}\omega_{i,3} - \sum_{h=1}^3 \omega_{i,h}(\frac{\omega_{i,h}}{l_{i,h}} + \dot{\beta}_{i,h}) + \frac{\epsilon_i^2 + 6}{2}e_{11}^2 \\ &\quad + \frac{\epsilon_i^2 + 6}{2}e_{12}^2 + \frac{\epsilon_i^2 + 3}{2}e_{13}^2 + c_1, \end{aligned} \tag{92}$$

where $\bar{\gamma}_1 = \frac{\gamma_1 + 1}{2}$, and $c_1 = \frac{k_{\Theta}}{2}\bar{\Theta}_i^T \bar{\Theta}_i + 0.2758\epsilon_{\rho} + 0.2758\epsilon_{\lambda} + \frac{\gamma_1^2}{2}f_{i,1}^2 + 0.2785\epsilon_f + \frac{1}{2}(f_{i,1}^2 + f_{i,2}^2) + \frac{1}{2}\bar{\omega}_{i,u}^2 + \frac{1}{2}\bar{\omega}_{i,r}^2 + 3(q_1^2 + q_2^2 + \frac{1}{2}q_3^2) + \frac{1}{2}\bar{a}_1 + \frac{1}{2}\bar{a}_2$.

Consider the total Lyapunov function as

$$V_2 = V_1 + V_o, \tag{93}$$

□

Remark 6. The Lyapunov function (V_1) includes estimation errors (e_{11}, e_{12}, e_{13}). We cannot conclude that $\dot{V}_1 \leq -c_0 V_1 + c_3$, c_0 and c_3 are positive constants. The Lyapunov function (V_2) is constructed by inducing V_o . In the time derivative of V_2 , the gain of estimation error is negative.

We can conclude that $\dot{V}_2 \leq -c_0V_2 + c_3$. Therefore, it is proven that all signals of the closed-loop system are bounded.

Along with (48) and (92), the time derivative of V_2 is

$$\begin{aligned} \dot{V}_2 \leq & -P_{ij}^TK_{i,1}P_{ij} - (k_{i,2} - \tilde{\gamma}_1)\psi_{i,e}^2 - (k_{i,3} - \frac{13}{2})u_{i,e}^2 \\ & - (k_{i,4} - 6)v_{i,e}^2 - (k_{i,5} - \frac{7}{2})r_{i,e}^2 - \frac{k_\Theta}{2}\tilde{\Theta}_i^T\tilde{\Theta}_i \\ & - (\bar{T}_u - \frac{1}{2})\alpha_{i,1}^2 - (\bar{T}_r - \tilde{\gamma}_1)\alpha_{i,3}^2 - f_i\omega_i \\ & + \psi_{i,e}\omega_{i,3} - \sum_{h=1}^3\omega_{i,h}(\frac{\omega_{i,h}}{l_{i,h}} + \dot{\beta}_{i,h}) \\ & - c_2\|E_t(t)\|^2 + c_1, \end{aligned} \tag{94}$$

where $c_2 = \frac{\varrho(1-c_{\varrho_1})}{2} - \frac{\epsilon_i^2+6}{2}$.

Define $\Omega_{i,1} = -f_{i,1} - \dot{\beta}_{i,1}$, $\Omega_{i,2} = -f_{i,2} - \dot{\beta}_{i,2}$ and $\Omega_{i,3} = \psi_{i,e} - \dot{\beta}_{i,3}$. According to Young’s inequality, $\omega_{i,h}\Omega_{i,h} \leq \frac{1}{2\varrho_c}\omega_{i,h}^2\Omega_{i,h}^2 + \frac{\varrho_c}{2}$. Then,

$$\begin{aligned} \dot{V}_2 \leq & -P_{ij}^TK_{i,1}P_{ij} - (k_{i,2} - \tilde{\gamma}_1)\psi_{i,e}^2 - (k_{i,3} - \frac{13}{2})u_{i,e}^2 \\ & - (k_{i,4} - 6)v_{i,e}^2 - (k_{i,5} - \frac{7}{2})r_{i,e}^2 - \frac{k_\Theta}{2}\tilde{\Theta}_i^T\tilde{\Theta}_i \\ & - (\bar{T}_u - \frac{1}{2})\alpha_{i,1}^2 - (\bar{T}_r - \tilde{\gamma}_1)\alpha_{i,3}^2 \\ & - \sum_{h=1}^3(\frac{\omega_{i,h}^2}{l_{i,h}} - \frac{\omega_{i,h}^2\Omega_{i,h}^2}{2\varrho_c}) - c_2\|E_t(t)\|^2 + c_3, \end{aligned} \tag{95}$$

where $c_3 = c_1 + \frac{3}{2}\varrho_c$, ϱ_c is a positive constant.

$|\Omega_{i,h}| \leq s_{i,h}$, $s_{i,h}$, $h = 1, 2, 3$ is a positive constant. $\frac{1}{l_{i,h}} = s_{i,h}^2/(2\varrho_c) + l_{i,h}^*$ with $l_{i,h}^* > 0$ is a constant. The follow can be attained:

$$\begin{aligned} \dot{V}_2 \leq & -P_{ij}^TK_{i,1}P_{ij} - (k_{i,2} - \tilde{\gamma}_1)\psi_{i,e}^2 - (k_{i,3} - \frac{13}{2})u_{i,e}^2 \\ & - (k_{i,4} - 6)v_{i,e}^2 - (k_{i,5} - \frac{7}{2})r_{i,e}^2 - \frac{k_\Theta}{2}\tilde{\Theta}_i^T\tilde{\Theta}_i \\ & - (\bar{T}_u - \frac{1}{2})\alpha_{i,1}^2 - (\bar{T}_r - \tilde{\gamma}_1)\alpha_{i,3}^2 \\ & - \sum_{h=1}^3l_{i,h}^*\omega_{i,h}^2 - \sum_{h=1}^3(1 - \frac{\Omega_{i,h}^2}{s_{i,h}^2})\frac{\omega_{i,h}^2s_{i,h}^2}{2\varrho_i} \\ & - c_2\|E_t(t)\|^2 + c_3, \end{aligned} \tag{96}$$

Owing to $|\Omega_{i,h}| \leq s_{i,h}$, the inequality (96) becomes

$$\dot{V}_2 \leq -c_0V_2 + c_3, \tag{97}$$

where $c_0 = \min\{2\lambda_{\min}(K_{i,1}), 2(k_{i,2} - \tilde{\gamma}_1), 2(k_{i,3} - \frac{13}{2}), 2(k_{i,4} - 6), 2(k_{i,5} - \frac{7}{2}), k_\Theta, 2(\bar{T}_u - \frac{1}{2}), 2(\bar{T}_r - \tilde{\gamma}_1), 2l_{i,h}^*, 2c_2/\lambda_{\max}(P)\}$.

Theorem 4. Zeno behavior can be avoided under the event-triggered mechanisms ((71) and (72)), and the implementation intervals $t_{k+1}^u - t_k^u$ and $t_{k+1}^r - t_k^r$ are lower-bounded by a positive constant (t^*).

Proof. According to (72),

$$\begin{cases} \frac{d}{dt}|e_u| = \text{sign}(e_u)\dot{e}_u \leq |\dot{\omega}_{\tau u}|, & \forall t \in [t_k^u, t_{k+1}^u) \\ \frac{d}{dt}|e_r| = \text{sign}(e_r)\dot{e}_r \leq |\dot{\omega}_{\tau r}|. & \forall t \in [t_k^r, t_{k+1}^r) \end{cases} \quad (98)$$

The time derivatives of $\omega_{\tau u}$ and $\omega_{\tau r}$ are expressed as

$$\dot{\omega}_{\tau u}(t) = m_{i,11}(-k_{i,3}\dot{u}_{i,e} + \ddot{\beta}_{i,1} - T_u\dot{\alpha}_{i,1} + \dot{f}_{i,1} - \dot{\hat{\sigma}}_{i,1}), \quad (99)$$

$$\dot{\omega}_{\tau r}(t) = m_{i,33}(-k_{i,5}\dot{r}_{i,e} + \ddot{\beta}_{i,3} - T_r\dot{\alpha}_{i,3} - \dot{\psi}_{i,e} - \dot{\hat{\sigma}}_{i,3}). \quad (100)$$

□

Theorem 3 shows that all signals in the closed-loop system are bounded. Therefore, $\dot{u}_{i,e}, \dot{r}_{i,e}, \ddot{\beta}_{i,1}, \ddot{\beta}_{i,3}, \dot{\alpha}_{i,1}, \dot{\alpha}_{i,3}$ and $\dot{\psi}_{i,e}$ are bounded. According to the design of the ETESO, $\hat{\sigma}_{i,1}$ and $\hat{\sigma}_{i,3}$ are bounded. $\dot{f}_{i,1}$ is bounded because $\|f_i\| \leq f_i^*$. Therefore, there are positive constants (k_u and k_r) satisfying $|\dot{\omega}_{\tau u}| \leq k_u$ and $|\dot{\omega}_{\tau r}| \leq k_r$. Since

$$\begin{cases} e_u(t_k^u) = 0, & \lim_{t \rightarrow t_{k+1}^u} |e_u(t)| = a_1 \\ e_r(t_k^r) = 0, & \lim_{t \rightarrow t_{k+1}^r} |e_r(t)| = a_2 \end{cases} \quad (101)$$

there exists a lower bound of implementation interval t^* and $t^* \geq \min\{a_1/k_u, a_2/k_r\}$. Hence, no Zeno phenomenon occurs when the proposed control law is used.

5. Simulation Results

In this section, simulation results are presented to prove the proposed event-triggered control method, and the ship parameters are chosen from [37]. Four USVs were driven to track a leader at a desired distance and angle with the proposed control law in (69)–(72). The total duration of the simulation runs was 120 s, and the sampling time t_s for each time point was 0.01 s. The initial positions of followers were chosen as $\eta_1(0) = [-2 \text{ m}, -5 \text{ m}, 0 \text{ rad}]^T$, $\eta_2(0) = [-2 \text{ m}, 5 \text{ m}, 0 \text{ rad}]^T$, $\eta_3(0) = [-4 \text{ m}, -8 \text{ m}, 0 \text{ rad}]^T$ and $\eta_4(0) = [-4 \text{ m}, 8 \text{ m}, 0 \text{ rad}]^T$. The trajectory of leader was generated by $u_j = 0.2 \text{ m/s}$, $v_j = 0 \text{ m/s}$ and $r_j = 0 \text{ rad/s}$ for $0 \leq t < 40 \text{ s}$; $u_j = 0.2 \text{ m/s}$, $v_j = 0 \text{ m/s}$ and $r_j = 0.1 \text{ rad/s}$ for $40 \text{ s} \leq t < 60 \text{ s}$; $u_j = 0.2 \text{ m/s}$, $v_j = 0 \text{ m/s}$ and $r_j = -0.1 \text{ rad/s}$ for $60 \text{ s} \leq t < 80 \text{ s}$; $u_j = 0.2 \text{ m/s}$, $v_j = 0 \text{ m/s}$ and $r_j = 0 \text{ rad/s}$ for $80 \text{ s} \leq t < 120 \text{ s}$; and $\eta_j(0) = [0 \text{ m}, 0 \text{ m}, 0 \text{ rad}]^T$. The desired distance and relative angle are expressed by $\rho_{1j,d} = 3 \text{ m}$, $\lambda_{1j,d} = 1 \text{ rad}$, $\rho_{2j,d} = 3 \text{ m}$, $\lambda_{2j,d} = -1 \text{ rad}$, $\rho_{3j,d} = 6 \text{ m}$, $\lambda_{3j,d} = 1 \text{ rad}$, $\rho_{4j,d} = 6 \text{ m}$ and $\lambda_{4j,d} = -1 \text{ rad}$.

The parameters of the ETESO were chosen as $\epsilon_i = 0.4$, $c_q = 0.1$. The parameters of the proposed control law were chosen as $\epsilon_f = 0.1$, $K_{\Theta} = \text{diag}\{5, 5\}$, $\gamma_{ij} = 0.001$, $K_{i,1} = \text{diag}\{5, 5\}$, $k_{i,2} = 5$, $k_{i,3} = 10$, $k_{i,4} = 10$, $k_{i,5} = 10$, $\gamma_1 = 5$, $T_u = 10$, $T_r = 16$, $l_{i,h} = 0.1$ and $h = 1, 2, 3$. The parameters of the trigger condition were $a_1 = a_2 = 0.2$.

Remark 7. According to inequality (97), we should keep c_0 as large as possible and c_3 as small as possible. A closed-loop system can converge quickly with small errors. However, c_3 includes the mismatch variables between input without saturation and input with saturation ($\bar{\omega}_{i,u}$ and $\bar{\omega}_{i,r}$). Large gain factors ($K_{i,1}$, $k_{i,2}$, $k_{i,3}$, $k_{i,4}$ and $k_{i,5}$) correspond to large mismatch variables. Therefore, gain factor was set as small as possible without violating the $c_0 > 0$ constraint. γ_1 , T_u and T_r define the convergence rate of auxiliary variables and satisfy the inequalities $T_u/\gamma_1 - 1/2 > 0$ and $T_r/\gamma_1 - (1 + \gamma_1)/2 > 0$. $l_{i,h}$ determines the tracking speed of the first-order filter, which is related to the sampling time of the simulation. An excessively large value results in an unstable system, and an excessively small value results in poor tracking performance. As a rule of thumb, the general recommended value of $l_{i,h}$ is between t_s and $10t_s$. The parameters a_1 and a_2 define the trigger condition of the proposed controller; larger a_1 and a_2 values indicate a lower update frequency of input signals and a poor system performance. To find a balance between update frequency and system performance, a_1 and a_2 are defined as $a_1 = a_2 = 0.2$. ϵ_i defines the estimation speed of the ETESO, c_q is the threshold of the trigger condition of the ETESO and the process of parameter

selection is similar to parameter selection in a_1 and a_2 . The ETESO and feed-forward compensation are relied upon, the influence of uncertainties is compensated immediately and the closed-loop system possesses strong robustness to different sets of parameters.

For surface vessels, the effect of gravity can be neglected because the gravity acting on USVs is equal to the buoyancy acting on USVs. USVs are subject to model uncertainties and environmental disturbances. Model uncertainties are induced by model errors and unknown system parameters. Therefore, only centrifugal terms, damping parameters and environmental disturbances are considered. In this paper, the uncertainties $\sigma_{i,1}$, $\sigma_{i,2}$ and $\sigma_{i,3}$ are assumed to be unknown. Environmental disturbances contain wind, wave and current information. The impacts on USVs of wind can be ignored due to a small windward area. Therefore, environmental disturbances are designed as the sum of some sinusoidal signals, which are chosen as $[0.18 - 0.18 \cos(0.01t)\cos(0.015t), 0.6 + 0.18 \sin(0.21t)\cos(0.2t), 0.6 - 0.18 \sin(0.2t)\cos(0.23t)]^T$.

Simulation results are shown in Figures 4–9. Figure 4 shows the formation pattern shaped by the five vessels; all followers can successfully track the leader. Figure 5 shows that the formation tracking errors approach zero, regardless of model uncertainties and environmental disturbances. Figure 6 shows the input signals of four USVs. In the first 24 s, since initial formation tracking errors are large, saturated control inputs suffer from sudden jumps. From 25 s to 40 s, formation tracking errors approach zero, and input signals convergence gradually. At 40s, 60s and 80s, sudden changes in the control forces are caused by a sudden change of the leader’s velocity.

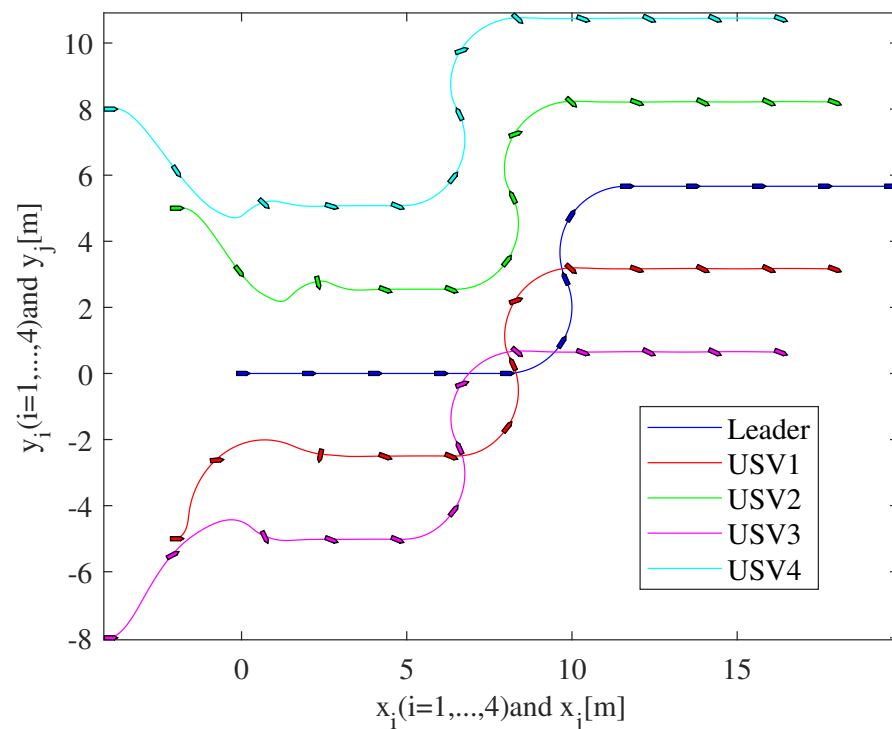


Figure 4. Formation pattern with four followers and a leader.

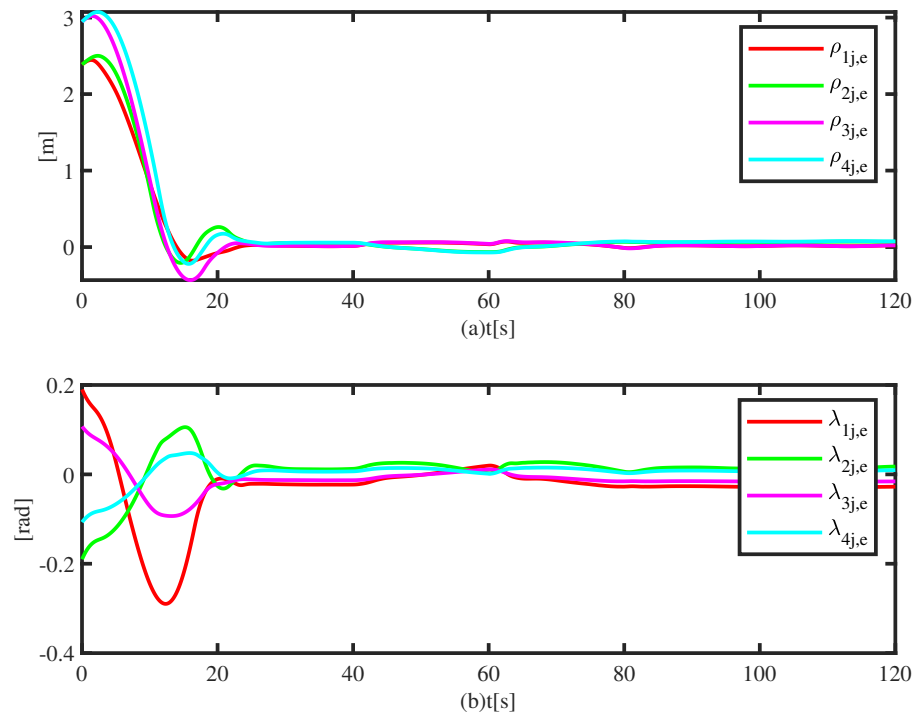


Figure 5. Tracking errors with perturbation effects.

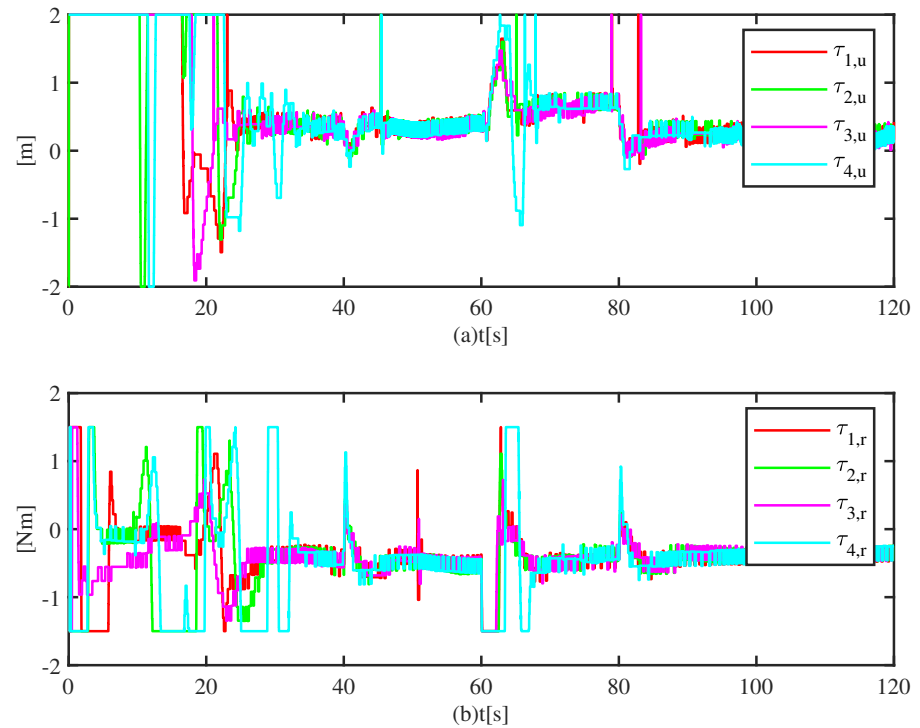


Figure 6. Input signals of four USVs.

Comparisons of simulation results are shown in Figures 7–9. Simulations were conducted using the TTETC proposed in [23] and the ETC proposed in this paper. The two controllers have same control parameters but different trigger condition parameters.

The TTETC was designed as follows:

$$\begin{cases} \tau_{i,uc}(t) = \omega_{\tau u}(t_k^u), & \forall t \in [t_k^u, t_{k+1}^u) \\ \tau_{i,rc}(t) = \omega_{\tau r}(t_k^r), & \forall t \in [t_k^r, t_{k+1}^r) \end{cases} \quad (102)$$

with

$$\begin{cases} t_k^u = \inf\{t \in \mathbb{R} | t > t_{k-1}^u \wedge e_u > \sigma V_2 \wedge V_2 > \mu\}, & t_1^u = 0 \\ t_k^r = \inf\{t \in \mathbb{R} | t > t_{k-1}^r \wedge e_r > (1 - \sigma)V_2 \wedge V_2 > \mu\}, & t_1^r = 0 \\ e_u = \omega_{\tau u} - \tau_{i,uc}, e_r = \omega_{\tau r} - \tau_{i,rc}, \end{cases} \quad (103)$$

$\mu = 0.02, \sigma = 0.5$.

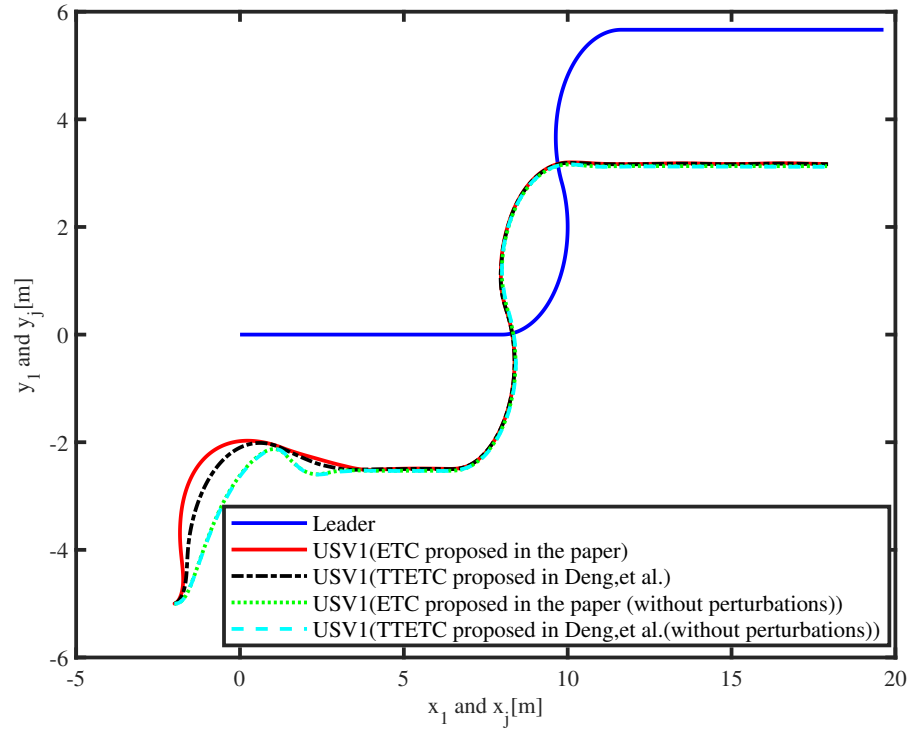


Figure 7. Leader–follower formation tracking control under four conditions, TTETC proposed in [23].

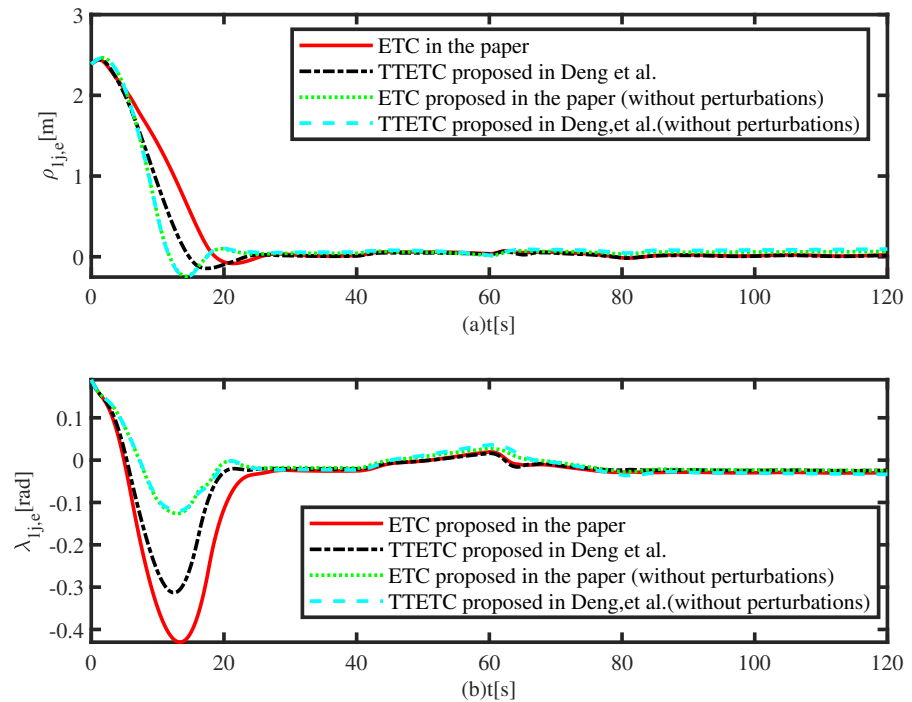


Figure 8. Tracking errors under different controllers, TTETC proposed in [23].

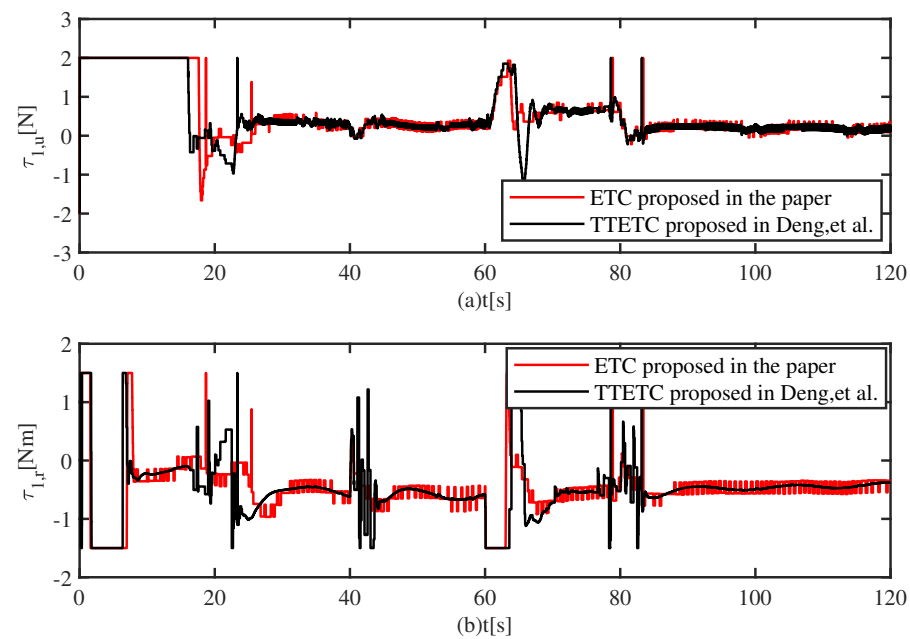


Figure 9. Control inputs with perturbation effects, TTETC proposed in [23].

Figure 7 depicts a formation pattern shaped by the i th USV and the leader. Different controllers are applied to the system with and without perturbations, revealing that the follower is able to track the leader successfully under four different conditions. Figure 8 depicts the distance and angle tracking errors under four different conditions, showing that the errors converge to the small neighborhood of the origin. Compared with the system with perturbations, the system without perturbations has a faster convergence rate. In the system with perturbations, some control energy is used to reject disturbances, including model uncertainties and environmental disturbances. Then, the energy that causes the system to converge is reduced. Under the same condition, the stability errors and convergence rates of the TTETC and ETC are nearly the same. The two controllers have the same structure but different event-triggered strategies. Therefore, they have the same convergence rate but different action times of the actuators. Figure 9 depicts the control signals generated by each of the controllers. Due to the effect of the proposed controller, the input signals shake at low frequencies, but their amplitudes are higher. At the beginning, due to a large initial formation tracking error, the input signals are saturated. The input signals converge, along with the convergence of formation tracking error. At 40 s, 60 s and 80 s, the input signals shake due to changes in the velocity of the leader. Figure 10 shows the control inputs within the first 20 s; the update frequencies of control inputs differ due to differing triggering strategies.

Figure 11 shows the event-based release instants and release intervals of input signals under the proposed controller. As shown in Table 2, compared with the TTETC, the proposed ETC largely reduces the action times of the actuators. The triggering condition of the TTETC was designed based on the Lyapunov function (V_2). In order to ensure the performance of control systems, the threshold is set to a smaller value. The threshold of the ETC was set to 0.2, and the action times of the actuators can be largely reduced.

The ESO was proposed in [31]. Figure 12 shows the estimated velocities and real velocities, illustrating that the velocity estimation of the ETESO is as good as that of the ESO. Figure 13 shows that the uncertainties are effectively approximated by the ESO and ETESO. Compared to the ESO, the ETESO simultaneously obtains a large steady error and a large jitter. Figure 14 shows the event-based release instants and release intervals of the ETESO; a locally enlarged drawing is also presented. From 40 to 45 s, the maximum release interval is 0.08, and the minimum release interval is 0.01. From 0 to 120 s, most release intervals are greater than 0.04. Therefore, some communication time is saved. Table 3 shows

the communication times of two observers. A counter was added in the simulation. When the event condition is met, the counter begins to count. After the application completes, the counter shows the total number of times the event occurred. Communication times can be attained by multiplying the total number of occurrences by the sampling time. Compared with the ESO, the ETESO can reduce communication costs and communication time. The ETESO is applied to reduce communication costs at the cost of lost estimation accuracy.

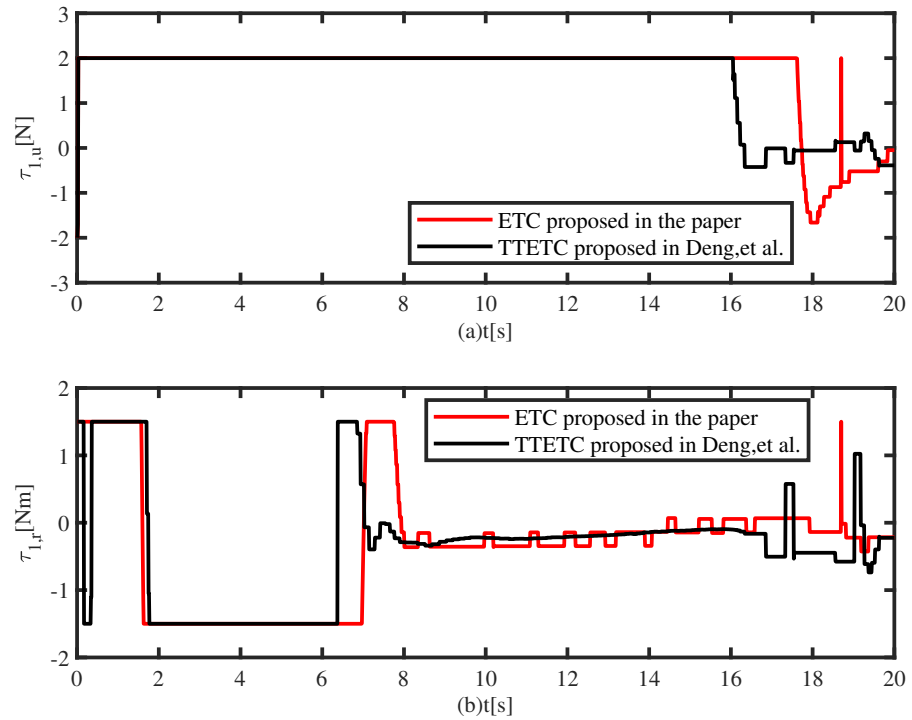


Figure 10. Locally enlarged diagram of Figure 9. TTETC proposed in [23].

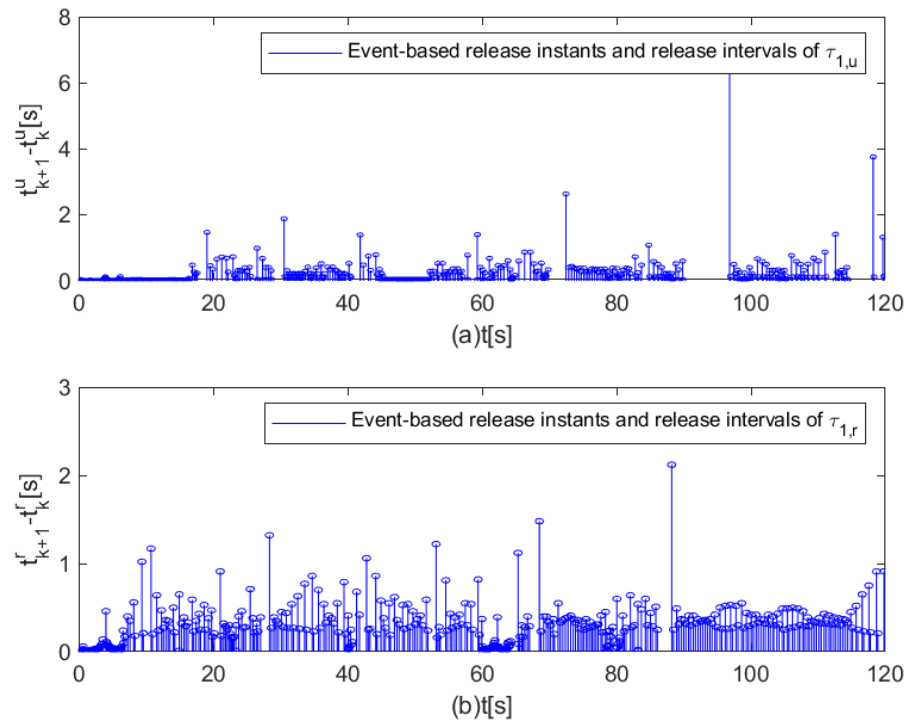


Figure 11. The event-based release instants and release intervals of input signals.

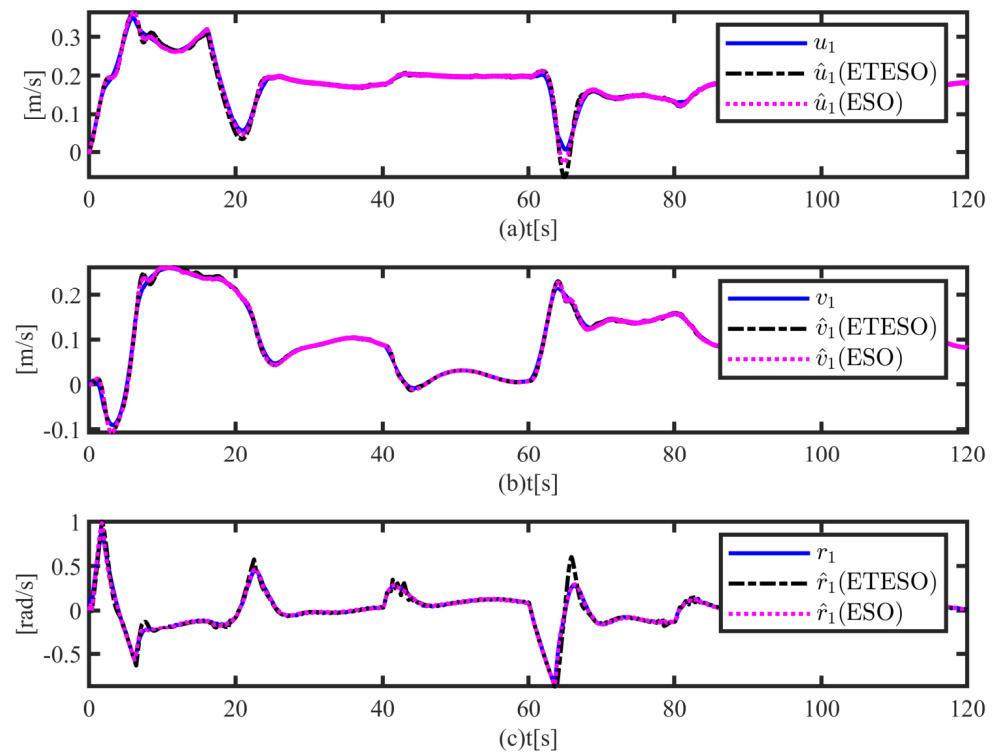


Figure 12. Comparisons of estimation performance.

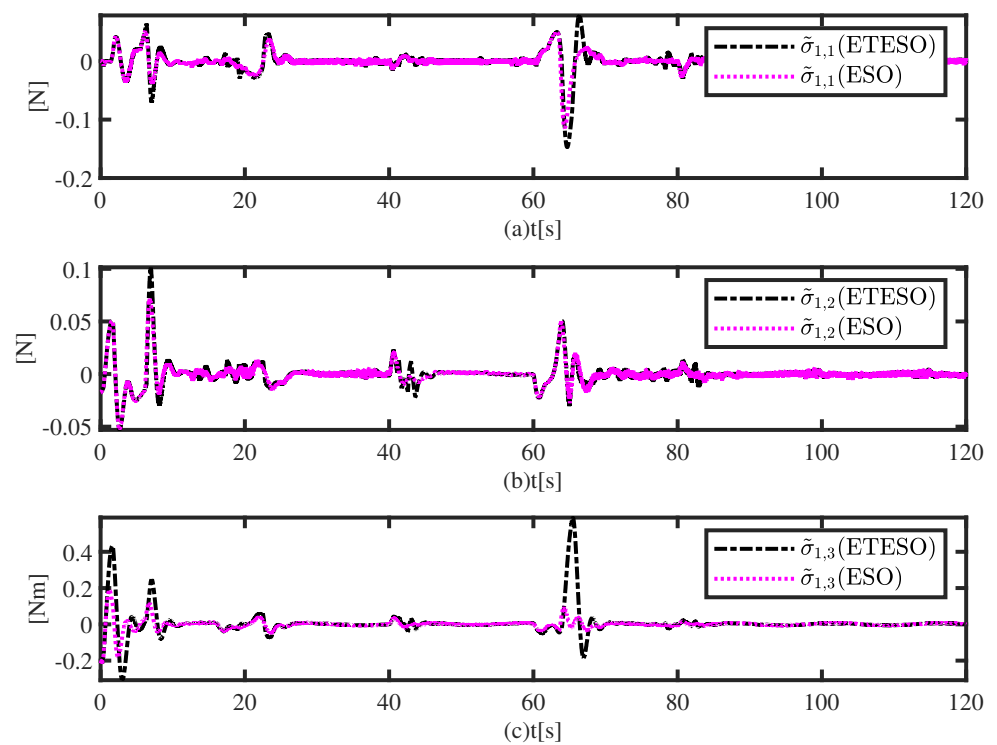


Figure 13. Approximation errors under different observers.

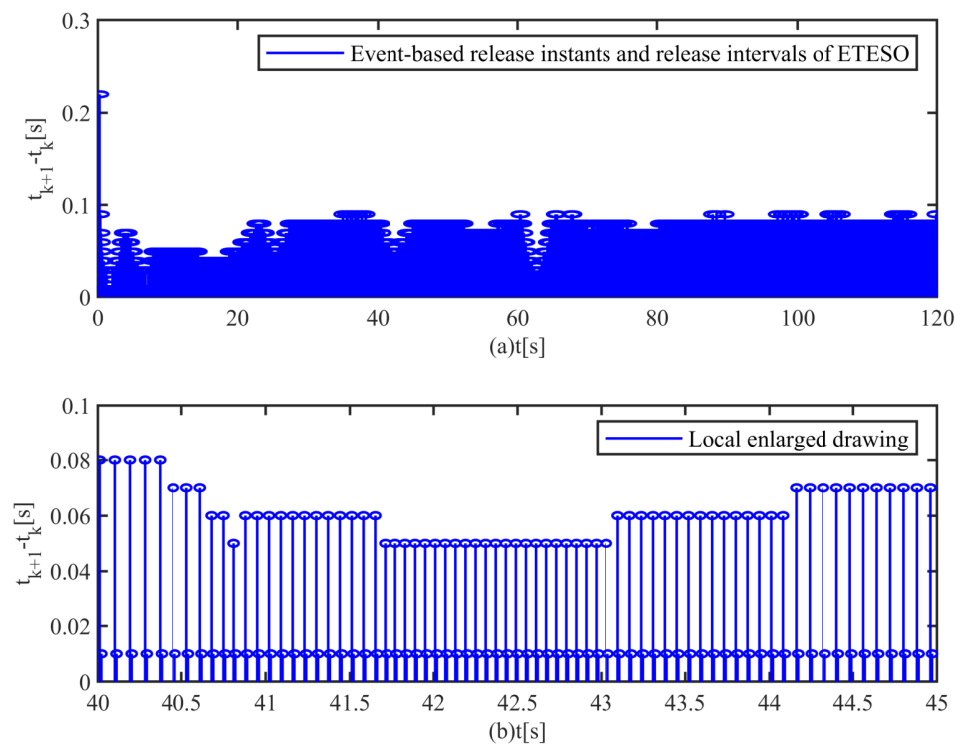


Figure 14. The triggering instants for the ETESO and its locally enlarged drawing.

Table 2. Comparisons of ETC and TTETC

Performance Parameter	ETC	TTETC
Convergent time	24.25 s	24.26 s
Convergent time (without perturbations)	24.21 s	24.22 s
Stability error $\rho_{1j,e}$	0.01 m	0.01 m
Stability error $\rho_{1j,e}$ (without perturbations)	0.01 m	0.01 m
Stability error $\lambda_{1j,e}$	−0.02 rad	−0.02 rad
Stability error $\lambda_{1j,e}$ (without perturbations)	−0.01 rad	−0.01 rad
Action times of $\tau_{1,uc}$	1321	2226
Action times of $\tau_{1,uc}$ (without perturbations)	1210	2064
Action times of $\tau_{1,rc}$	702	2226
Action times of $\tau_{1,rc}$ (without perturbations)	504	2064

Table 3. Comparisons of communication time.

Serial Number	Variable	Time (s)
(1)	ETESO	31.84
(2)	ESO	120

6. Conclusions

This article suggests an output feedback controller for surface vessels with model uncertainties, unknown environmental disturbances and input constraints. An ETESO was proposed, and unknown model dynamics and velocity were simultaneously estimated. The controller was designed based on the ETESO. Finally, a mathematical analysis was conducted, proving that all error signals of the system are bounded. Simulation experiments affirm the tracking performance of the proposed controller. When USVs start tracking formation, the control inputs suffer from sudden jumps. The design of an active collision avoidance system is one of the core issues in the area of the formation tracking control of USVs. To solve this problem, smooth avoidance path planing approaches can be considered in future works.

Author Contributions: Conceptualization, methodology, software and writing—review and editing, X.X.; validation, Z.Y.; writing—review and editing, T.Y. All authors have read and agreed to the published version of the manuscript.

Funding: This research received no external funding.

Institutional Review Board Statement: This article does not contain any studies involving human or animal subjects.

Data Availability Statement: The data reported in this paper are unavailable.

Conflicts of Interest: The authors declare no conflict of interest.

References

1. Peng, Z.; Wang, J.; Wang, D.; Han, Q.L. An Overview of Recent Advances in Coordinated Control of Multiple Autonomous Surface Vehicles. *IEEE Trans. Ind. Inform.* **2021**, *17*, 732–745. [[CrossRef](#)]
2. Tran, Q.V.; Lee, C.; Kim, J.; Nguyen, H.Q. Robust Bearing-Based Formation Tracking Control of Underactuated Surface Vessels: An Output Regulation Approach. *IEEE Trans. Control. Netw. Syst.* **2023**, 1–12. [[CrossRef](#)]
3. Yoo, S.J.; Park, B.S. Approximation-Free Design for Distributed Formation Tracking of Networked Uncertain Underactuated Surface Vessels under Fully Quantized Environment. *Nonlinear Dyn.* **2023**, *111*, 6411–6430. [[CrossRef](#)]
4. Cui, R.; Ge, S.; How, B.; Choo, Y. Leader–Follower Formation Control of Underactuated Autonomous Underwater Vehicles. *Ocean. Eng.* **2010**, *37*, 1491–1502. [[CrossRef](#)]
5. Xia, G.; Xia, X.; Zhao, B.; Sun, C.; Sun, X. A Solution to Leader Following of Underactuated Surface Vessels with Actuator Magnitude and Rate Limits. *Int. J. Adapt. Control. Signal Process.* **2021**, *35*, 1860–1878. [[CrossRef](#)]
6. Beard, R.; Lawton, J.; Hadaegh, F. A Coordination Architecture for Spacecraft Formation Control. *IEEE Trans. Control. Syst. Technol.* **2001**, *9*, 777–790. [[CrossRef](#)] [[PubMed](#)]
7. Park, B.S.; Yoo, S.J. An Error Transformation Approach for Connectivity-Preserving and Collision-Avoiding Formation Tracking of Networked Uncertain Underactuated Surface Vessels. *IEEE Trans. Cybern.* **2019**, *49*, 2955–2966. [[CrossRef](#)] [[PubMed](#)]
8. Wang, H.; Luo, Q.; Li, N.; Zheng, W. Data-Driven Model Free Formation Control for Multi-USV System in Complex Marine Environments. *Int. J. Control. Autom. Syst.* **2022**, *20*, 3666–3677. [[CrossRef](#)]
9. Liu, H.; Weng, P.; Tian, X.; Mai, Q. Distributed Adaptive Fixed-Time Formation Control for UAV-USV Heterogeneous Multi-Agent Systems. *Ocean. Eng.* **2023**, *267*, 113240. [[CrossRef](#)]
10. Wu, W.; Tong, S. Collision-Free Adaptive Fuzzy Formation Control for Unmanned Surface Vehicle Systems with Input Saturation. *Int. J. Fuzzy Syst.* **2023**. [[CrossRef](#)]
11. Chen, M.; Ge, S.S.; How, B.V.E.; Choo, Y.S. Robust Adaptive Position Mooring Control for Marine Vessels. *IEEE Trans. Control. Syst. Technol.* **2013**, *21*, 395–409. [[CrossRef](#)]
12. Shojaei, K. Leader–Follower Formation Control of Underactuated Autonomous Marine Surface Vehicles with Limited Torque. *Ocean. Eng.* **2015**, *105*, 196–205. [[CrossRef](#)]
13. Park, B.S.; Kwon, J.W.; Kim, H. Neural Network-Based Output Feedback Control for Reference Tracking of Underactuated Surface Vessels. *Automatica* **2017**, *77*, 353–359. [[CrossRef](#)]
14. Xia, G.; Xia, X.; Zhao, B.; Sun, C.; Sun, X. Distributed Tracking Control for Connectivity-Preserving and Collision-Avoiding Formation Tracking of Underactuated Surface Vessels with Input Saturation. *Appl. Sci.* **2020**, *10*, 3372. [[CrossRef](#)]
15. Deng, Y.; Zhang, X.; Im, N.; Zhang, G.; Zhang, Q. Adaptive Fuzzy Tracking Control for Underactuated Surface Vessels with Unmodeled Dynamics and Input Saturation. *ISA Trans.* **2020**, *103*, 52–62. [[CrossRef](#)] [[PubMed](#)]
16. Xia, G.; Xia, X.; Sun, X. Formation Control with Collision Avoidance for Underactuated Surface Vehicles. *Asian J. Control.* **2021**, *24*, 2244–2257. [[CrossRef](#)]
17. Liu, C.; Chen, C.L.P.; Zou, Z.; Li, T. Adaptive NN-DSC Control Design for Path Following of Underactuated Surface Vessels with Input Saturation. *Neurocomputing* **2017**, *267*, 466–474. [[CrossRef](#)]
18. Zhang, B.; Xia, G. Output Feedback Tracking Control with Collision Avoidance for Dynamic Positioning Vessel under Input Constraint. *J. Mar. Sci. Eng.* **2023**, *11*, 811. [[CrossRef](#)]
19. Xia, G.; Xia, X.; Bo, Z.; Sun, X.; Sun, C. Event-Triggered Controller Design for Autopilot with Input Saturation. *Math. Probl. Eng.* **2020**, *2020*, e5362895. [[CrossRef](#)]
20. von Ellenrieder, K.D. Dynamic Surface Control of Trajectory Tracking Marine Vehicles with Actuator Magnitude and Rate Limits. *Automatica* **2019**, *105*, 433–442. [[CrossRef](#)]
21. Xia, G.; Xia, X.; Zheng, Z. Formation tracking control for underactuated surface vehicles with actuator magnitude and rate saturations. *Ocean. Eng.* **2022**, *260*, 111935. [[CrossRef](#)]
22. Wang, S.; Gao, Y.; Liu, J.; Wu, L. Saturated Sliding Mode Control with Limited Magnitude and Rate. *IET Control. Theory Appl.* **2018**, *12*, 1075–1085. [[CrossRef](#)]
23. Deng, Y.; Zhang, X.; Im, N.; Zhang, G.; Zhang, Q. Event-Triggered Robust Fuzzy Path Following Control for Underactuated Ships with Input Saturation. *Ocean. Eng.* **2019**, *186*, 106122. [[CrossRef](#)]

24. Xia, G.; Zheda, R. Event-triggered fixed-time distributed output feedback sliding mode cooperative control for multiple surface vessels with input saturation. *Trans. Inst. Meas. Control.* **2023**. . [[CrossRef](#)]
25. Peng, Z.; Jiang, Y.; Wang, J. Event-Triggered Dynamic Surface Control of an Underactuated Autonomous Surface Vehicle for Target Enclosing. *IEEE Trans. Ind. Electron.* **2021**, *68*, 3402–3412. [[CrossRef](#)]
26. Ahmad, I.; Ouannas, A.; Shafiq, M.; Pham, V.T.; Baleanu, D. Finite-Time Stabilization of a Perturbed Chaotic Finance Model. *J. Adv. Res.* **2021**, *32*, 1–14. [[CrossRef](#)] [[PubMed](#)]
27. Sun, Z.; Zhang, G.; Lu, Y.; Zhang, W. Leader-Follower Formation Control of Underactuated Surface Vehicles Based on Sliding Mode Control and Parameter Estimation. *ISA Trans.* **2018**, *72*, 15–24. [[CrossRef](#)] [[PubMed](#)]
28. Ahmad, I.; Shafiq, M. Oscillation Free Robust Adaptive Synchronization of Chaotic Systems with Parametric Uncertainties. *Trans. Inst. Meas. Control.* **2020**, *42*, 1977–1996. [[CrossRef](#)]
29. Jin, X. Fault Tolerant Finite-Time Leader–Follower Formation Control for Autonomous Surface Vessels with LOS Range and Angle Constraints. *Automatica* **2016**, *68*, 228–236. [[CrossRef](#)]
30. Peng, Z.h.; Wang, D.; Lan, W.y.; Sun, G. Robust Leader-Follower Formation Tracking Control of Multiple Underactuated Surface Vessels. *China Ocean. Eng.* **2012**, *26*, 521–534. [[CrossRef](#)]
31. Peng, Z.; Wang, D.; Li, T.; Han, M. Output-Feedback Cooperative Formation Maneuvering of Autonomous Surface Vehicles With Connectivity Preservation and Collision Avoidance. *IEEE Trans. Cybern.* **2020**, *50*, 2527–2535. [[CrossRef](#)]
32. Lu, Y.; Zhang, G.; Qiao, L.; Zhang, W. Adaptive Output-Feedback Formation Control for Underactuated Surface Vessels. *Int. J. Control.* **2020**, *93*, 400–409. [[CrossRef](#)]
33. Liu, L.; Zhang, W.; Wang, D.; Peng, Z. Event-Triggered Extended State Observers Design for Dynamic Positioning Vessels Subject to Unknown Sea Loads. *Ocean. Eng.* **2020**, *209*, 107242. [[CrossRef](#)]
34. Yu, Y.; Yuan, Y.; Yang, H.; Liu, H. A Novel Event-Triggered Extended State Observer for Networked Control Systems Subjected to External Disturbances. *Int. J. Robust Nonlinear Control.* **2019**, *29*, 2026–2040. [[CrossRef](#)]
35. Do, K.; Jiang, Z.; Pan, J. Underactuated Ship Global Tracking under Relaxed Conditions. *IEEE Trans. Autom. Control.* **2002**, *47*, 1529–1536. [[CrossRef](#)]
36. Polycarpou, M. Stable Adaptive Neural Control Scheme for Nonlinear Systems. *IEEE Trans. Autom. Control.* **1996**, *41*, 447–451. [[CrossRef](#)]
37. Skjetne, R.; Fossen, T.I.; Kokotović, P.V. Adaptive Maneuvering, with Experiments, for a Model Ship in a Marine Control Laboratory. *Automatica* **2005**, *41*, 289–298. [[CrossRef](#)]

Disclaimer/Publisher’s Note: The statements, opinions and data contained in all publications are solely those of the individual author(s) and contributor(s) and not of MDPI and/or the editor(s). MDPI and/or the editor(s) disclaim responsibility for any injury to people or property resulting from any ideas, methods, instructions or products referred to in the content.